NASA TECHNICAL NOTE

NASA TN D-2839

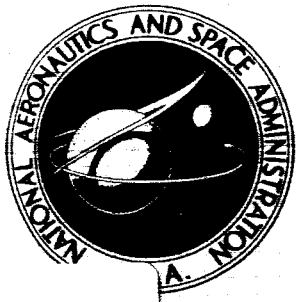

DESIGN ANALYSIS AND GENERAL CHARACTERISTICS OF FLAT-PLATE CENTRAL-FIN-TUBE SENSIBLE-HEAT SPACE RADIATORS

by Arthur V. Saule, Richard P. Krebs, and Bruce M. Auer

Lewis Research Center

Cleveland, Ohio

NATIONAL AERONAUTICS AND SPACE ADMINISTRATION • WASHINGTON, D. C. • JUNE 1965

NASA TN D-2839

DESIGN ANALYSIS AND GENERAL CHARACTERISTICS OF FLAT-PLATE CENTRAL-FIN-TUBE SENSIBLE-HEAT SPACE RADIATORS

By Arthur V. Saule, Richard P. Krebs, and Bruce M. Auer

Lewis Research Center
Cleveland, Ohio

NATIONAL AERONAUTICS AND SPACE ADMINISTRATION

For sale by the Clearinghouse for Federal Scientific and Technical Information
Springfield, Virginia 22151 – Price $3.00

CONTENTS

DESIGN ANALYSIS AND GENERAL CHARACTERISTICS OF FLAT-PLATE CENTRAL-FIN-TUBE SENSIBLE-HEAT SPACE RADIATORS

by Arthur V. Saule, Richard P. Krebs, and Bruce M. Auer

Lewis Research Center

SUMMARY

An analysis is reported for the calculation of the characteristics, performance, weight, and area of a single-panel flat-plate central-fin-tube sensible-heat space radiator for a set of thermodynamic and fluid-mechanic conditions. The analysis takes into account the axial temperature gradient and the change in fin-tube effectiveness along the tube and fin.

An example for each type of working fluid (liquid metal, liquid, and inert gas) is discussed in detail. The three examples were selected from representative applications to typical Rankine and Brayton cycle space power-generation systems as well as to secondary cooling loops. Examples show how changes in geometric parameters, mass flow rates, working fluids, and flow regimes (turbulent or laminar) affect the radiator weight and panel planform area.

Particular examples indicate that there are unique ranges of geometric parameters (fin-tube profile ratio, initial conductance parameter, and tube inside diameter) for minimum weight radiators. The magnitudes of these parameters depend on the phase of the working fluid (gaseous or liquid), flow regimes, and other operating conditions.

INTRODUCTION

There are many applications for a heat-rejection device in space. Vehicle cabins will have to be conditioned, equipment and instruments will have to be cooled, and the waste heat from power-generating systems will have to be expelled. As the payloads become heavier and the missions longer, the cooling loads and the electric power requirements become greater. As a result, the thermal radiator, or heat-rejecting device, also becomes larger. In fact, the radiator may become one of the largest and heaviest components of a space powerplant (e.g., ref. 1).

Because the radiator is so large, it must be carefully designed to minimize the size or weight while maintaining its thermodynamic and structural requirements and fluid-mechanic performance in the space environment. The design of a condenser-radiator, in which the working fluid changes from a vapor to a liquid within the radiator, has been discussed in considerable detail in the literature (e.g., refs. 2 to 9). However, papers dealing with the

sensible-heat radiator, in which the working fluid maintains its phase (gas or liquid), but loses sensible heat and temperature, are less numerous (refs. 10 to 14). In most of these papers the radiator was considered to be constructed with a central-fin-tube geometry, in which the tubes carrying the working fluid are separated by rectangular heat-conducting and -radiating fins.

Radiators that use a single-phase working fluid may be employed, for example, for the Rankine vapor cycle where a heat exchanger similar to the shell and tube type, called a heat-exchanger - condenser, is used to condense the vapor. Subcooled liquid is provided for the condenser by a circuit that passes through an all-liquid radiator (ref. 1). As another application, sensible-heat radiators are also considered for secondary cooling systems such as coolant circuits required by space environmental control and component cooling systems (ref. 14). In this report, secondary cooling means any cooling other than rejection of waste heat from power cycles. Finally, probably one of the most important uses for the sensible-heat radiator is in a Brayton cycle (ref. 15), where a radiator that employs an inert gas as the working fluid may be directly coupled to a gas recuperator or a cooling loop with a gas-liquid heat exchanger and a radiator with liquid as the working fluid may be added to the system.

Part of the dearth of analyses for the sensible-heat radiator may be attributed to the increased thermodynamic complexity of this radiator over the condenser-radiator. The simultaneous temperature gradients, both axially along the tube and the fin and perpendicularly through the fin, cause the temperature to be at least two dimensional everywhere in the radiator. This complication renders the condenser-radiator analysis inadequate for the sensible-heat radiator unless the axial temperature drop is very small compared with the terminal temperature (ref. 11).

While reference 10 affords a means of determining or analyzing the performance of a given radiator under variable ambient conditions, it does not give a direct approach to radiator design to meet specific heat-rejection requirements. Furthermore, reference 11 requires a restriction on the fin geometry (constant-temperature-gradient fin, or fins with root thickness equal to the outside tube diameter) if the temperature drop in the working fluid is large. Neither report considers the design or performance of the headers at either end of the radiator tubes. Similarly, reference 12 does not show a header analysis and neglects solar and other incident radiation such as thermal radiation from nearby planets and adjacent vehicle components. Reference 12 has developed a simplified method for optimizing a rectangular fin, but it assumes geometric view factors for fin and tube equal to 1. The tube wall thickness, furthermore, is selected to satisfy structural requirements alone without consideration of meteoroid penetration.

In addition to flat-plate central-fin-tube sensible-heat space radiators, literature is also available on cyclindrical radiators with internally located tubes, where the thermal radiation is considered from the convex side alone. Representing such radiators are, for example, references 13 and 14. Reference 13 assumes a constant fin effectiveness and tube wall thickness not determined from present meteoroid penetration theory. It also neglects incident thermal radiation and headers. Reference 14 considers low-temperature laminar-

flow fluids, and presents a verification of the results of the analysis by appropriate experiments. It appears, however, that this method may be more applicable to analyzing the performance of a given radiator and less adaptable to designing a radiator that has to satisfy certain inlet and outlet conditions of temperature and pressure when the heat-rejection rate is fixed.

To fulfill the need for a more comprehensive and flexible fin-tube sensible-heat-radiator design procedure covering a wide range of design conditions, the Lewis Research Center developed the analysis discussed herein. It is applicable for designing flat-plate central-fin-tube radiators that use liquid metal, liquid, and inert gas as working fluids either in laminar or turbulent flow. It includes an analysis of the headers and takes into account the effect of the solar and all other incident radiation by an equivalent sink temperature. The tube and header wall thickness is determined by applying the latest concepts in meteoroid protection theory. Rather than using an average fin efficiency for the entire radiator, the method discussed in this report introduces a variable fin-tube effectiveness, which includes radiation interchange between fins and tubes, and thus accounts for axial and lateral temperature changes. The solution is accomplished by a numerical step-by-step procedure.

Details of the analysis, equations, and procedures are presented, and some of the thermal and geometric characteristics of flat-plate central-fin-tube sensible-heat radiators are demonstrated. Three examples were chosen, one for each type of working fluid: liquid metal, liquid, and inert gas. The examples were taken from representative applications to typical Rankine and Brayton cycle space power-generation systems as well as to secondary cooling loops. In addition, an application of the flat-plate central-fin-tube radiator to multiple-panel arrangements is discussed.

ANALYSIS

Approach

The analysis used in this report was developed specifically for a single-panel central-fin-tube flat-plate radiator emitting from both surfaces, similar to the one shown in figure 1. The working fluid enters the radiator through an inlet header that distributes the working fluid to evenly spaced, straight, circular, noninternally finned tubes. These tubes are all of the same length and diameter and are separated by rectangular fins. In passing through the tubes, the working fluid is cooled ultimately by thermal radiation from the outer surfaces of the tubes and fins. At the discharge end of the tubes the fluid is collected into an outlet header.

The shape and size of the headers depend on the phase of the fluid. The tapered headers shown in figure 1(a) resemble those where gas is used as the radiator working fluid. In this configuration, the gas is taken into the inlet header at one side of the radiator and leaves the outlet header at the opposite side of the radiator panel. It was assumed that this arrangement may approach equal pressure drop across each tube and thereby promote uniform flow distribution, similar velocity profiles in both headers, and equal tube lengths. The

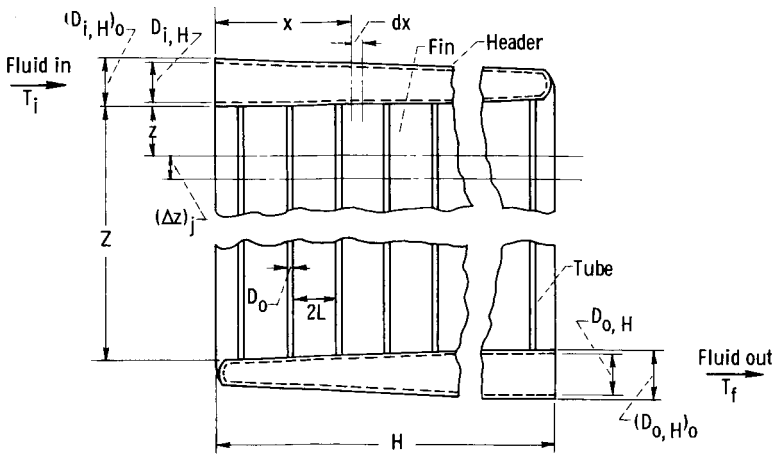

(a) Gas working fluid.

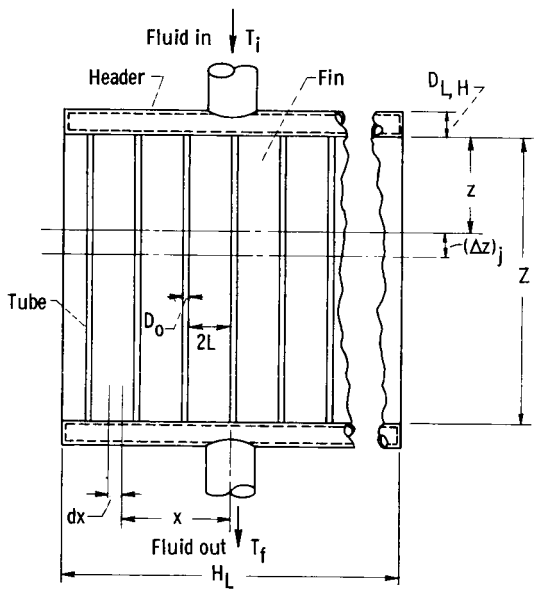

(b) Liquid working fluid.

Figure 1. - Radiator panel and header arrangement.

headers for liquids or liquid metals, because of their relatively small size, were assumed to have constant diameters, as shown in figure 1(b).

The objective of the analysis is to generate a radiator geometry that meets the design thermodynamic, fluid-mechanics, and environmental requirements and to determine the radiator panel planform area and weight. This objective has been accomplished in reference 5 for a direct-condensing radiator in which the temperature of the tube surface and fin base was nearly constant in the direction of fluid flow. The temperature gradient in the fin in a direction perpendicular to the tube axis and the radiant interchange between fin and tube, and between adjacent tubes, was accounted for by an overall fin and tube effectiveness in that reference.

The heat-transfer analysis for the sensible-heat radiator with which this report is concerned is inherently more complicated than for the direct-condensing radiator because of the additional temperature gradient in the tube axial direction. To circumvent this difficulty the sensible-heat radiator is assumed to be divided into strips perpendicular to the tube axis. These strips are then assumed to be isothermal, and an analysis for thermal radiation similar to that described in reference 5 is applied to each strip. The heat radiation rate for the entire radiator is then equal to the sum of the heat radiation rates from each strip. The number of strips used is dependent on the required accuracy in the heat transfer.

The general approach to the radiator design begins with the determination of the fin and tube geometry in the radiator panel. This geometry is dependent on the heat-transfer characteristics, the meteoroid-protection requirements, and the pressure drop prescribed for the tube. The heat-transfer analysis takes into account the effect of the temperature drop between the working fluid and the tube wall and the temperature drop through the tube armor as well as the temperature gradients and radiant interchange previously discussed. The effects of incident radiation from such sources as the Sun, nearby planets, or objects adjacent to the radiator are incorporated into an equivalent sink temperature (e.g., ref. 16). Details and the derivation of the heat-transfer analysis are given in the succeeding section of this report, and all symbols used are defined in appendix A.

The analysis of the meteoroid protection requirements is based on reference 17 and is given in appendix B. The pressure drop analysis can be found in appendix C. The tube and fin geometry and the panel planform area are calculated from the equations given in appendix D.

After the panel has been designed, the shape and weight of the headers are found in accordance with the analysis in appendix E. The maximum diameter of the headers is determined so that the pressure drop in the header will be a prescribed value for a header length equal to the panel width. The heat radiated from the headers is assumed to be negligible compared with the total heat-rejection rate from the radiator. This assumption has also been checked in appendix E and is shown to be the case providing that the prescribed pressure drop in the headers will minimize the total radiator weight for a given tube inside diameter, fin-tube profile ratio, and initial conductance parameter. The analysis is completed after the total and component weights of the radiator have been determined from the equations in appendix F.

In order to make the radiator-design calculations, certain inputs are required. These include the radiator heat load, expressed in terms of the inlet and exit temperatures T_i and T_f, respectively, mass flow rate $\dot{m}$, and specific heat of the working fluid c_p. Other inputs required are the allowable pressure drop in each header $(\Delta P)_{i,H}$ and $(\Delta P)_{o,H}$, the pressure drop in the tubes $(\Delta P)_t$, and for those radiators in which a gas is the working fluid, the pressure level P_i. It is also necessary to specify the sink temperature T_s and the constants describing the meteoroid penetration phenomenon (see appendix B). Three parameters describing the fin and tube geometry (the tube inside diameter D_{in}, the ratio of the half-fin width to the tube outside radius L/R_o,

and the so-called fin conductance parameter λ_1, e.g., ref. 5, at the inlet of the tubes) are also input variables. Physical and thermal properties of the working fluid and radiator material such as the thermal conductivity k, the viscosity μ, the density ρ, the gas constant R, and the hemispherical emissivity ϵ, complete the quantities that must be supplied.

The outputs consist chiefly of component dimensions and weights. These include the number of tubes N, the length of the tubes Z, the armor thickness δ_a, the outside tube diameter D_o, the fin thickness t, the panel planform area A_P, the vulnerable area of the tubes $A_{t,v}$, the maximum inside diameter of the inlet and outlet headers $D_{i,H}$ and $D_{o,H}$, respectively, and the total vulnerable area of the two headers $A_{H,v}$. The weights include the total radiator weight W_r, fin weight W_F, tube weight W_t, header weight (W_H for gases or $W_{L,H}$ for liquids), and liquid content weight W_I for liquids. Other outputs include the inside film and overall heat-transfer coefficients h_{in} and U_o, respectively, the fluid velocity at the inlet to the tube V_i, and the average Reynolds number in the tube Re.

Although the procedure was written for a single-panel radiator configuration, it can also be used to design one unit of a segmented radiator having $\bar{p}$ identical segments in which all segments are either interconnected or isolated, providing that there is no radiant interchange among the individual segments and that no segment acts as a shield for meteoroids for any other segment. If all segments are interconnected, that is, if the failure of any single segment will render the entire radiator inoperative, then one of the $\bar{p}$ segments of a radiator having a flow rate $\dot{m}$ and an overall probability of no meteoroid penetration equal to $P(0)$ can be designed by using a mass flow rate of $\dot{m}/\bar{p}$ and a probability $p(0) = P(0)^{1/\bar{p}}$ as inputs to the computer program described herein. On the other hand, if all segments can be isolated, that is, if only the punctured segments become inoperative, then the probability of no meteoroid penetration of a single panel $p(0)$ is obtained from the cumulative binomial distribution function

$$P(0) = \sum_{r=\bar{p}_s}^{\bar{p}} \frac{\bar{p}!}{r!(\bar{p} - r)!} \left[1 - p(0)\right]^{\bar{p}-r} \left[p(0)\right]^r$$

where $P(0)$ is the probability of having $\bar{p}_s$ or more segments not punctured and $p(0)$ is the probability of each of $\bar{p}$ identical segments. The mass flow rate in each of these $\bar{p}$ segments, however, is calculated the same way as for interconnected segments.

Heat Transfer

The net heat transfer in sensible-heat radiators can be solved by simplified numerical methods if isothermal radiant interchange and no axial heat conduction are approximated locally (ref. 18). The method adopted herein divides

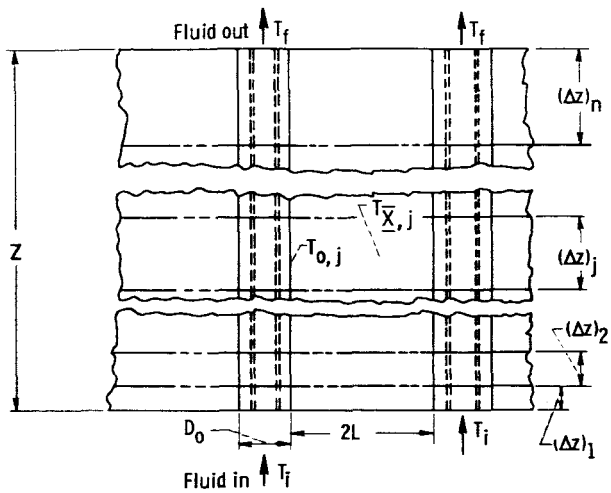

(a) Planform section of radiator panel.

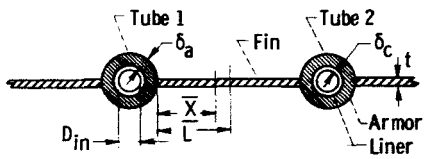

(b) Typical cross section.

Figure 2. - Schematic drawing of radiator panel showing isothermal strips used for numerical analysis.

the radiator panel into a number of elemental strips, each of which is assumed to be isothermal as shown in figure 2. The length of each strip is chosen so that each strip radiates heat at the same rate. This implies that the temperature drop of the fluid in each strip is the same, but the incremental length $(\Delta z)_j$ varies. The steady-state energy balance is now written for each strip in a step-by-step procedure. Assumptions adopted in various phases of the development are indicated in the process of the analysis.

Convection and conduction. - The loss of the sensible heat of the fluid in any elemental strip for all tubes is

$$\Delta Q_S = 3600\dot{m}c_p \Delta T = \text{const} \qquad (1)$$

where

$$\Delta T = \frac{T_i - T_f}{n} = \text{const} \qquad (2)$$

In this analysis it is assumed that the flow rate $\dot{m}$, specific heat c_p, fluid temperatures at the inlet T_i and at the exit T_f, and the number of the elements n are known quantities.

The sensible-heat energy, in turn, is transferred to the inside surface of the tubes by convection and to the outside surface of the tubes by conduction. In terms of an overall heat-transfer coefficient,

$$(\Delta Q_C)_j = U_o(\Delta A_t)_j(T_j - T_{o,j}) \qquad (3)$$

where

$$(\Delta A_t)_j = \pi D_o N(\Delta z)_j$$

is the tube outside surface area of any radiator element j. The fluid temperature T_j represents the average fluid bulk temperature in the tube element j and is obtained from the known inlet temperature T_i and ΔT as

$$T_j = T_i - \Delta T(j - 0.5) \qquad (4)$$

The overall heat-transfer coefficient based on the outside tube area in

equation (3) is obtained from the relation

$$U_o = \frac{1}{\frac{\frac{D_o}{D_{in}}}{3600h_{in}} + \frac{D_o \ln \frac{D_o}{D_{in}}}{2k_t}} \tag{5a}$$

where h_{in} is the average film coefficient of heat transfer, and the constant 3600 is used to make units of h_{in} and U_o consistent. If it can be assumed that the radial temperature drop in the tube walls is negligible, that is,

$$\frac{D_o \ln \frac{D_o}{D_{in}}}{2k_t} \ll \frac{\frac{D_o}{D_{in}}}{3600h_{in}}$$

equation (5a) becomes

$$U_o = 3600h_{in} \frac{D_{in}}{D_o} \tag{5b}$$

Equation (5b) may be used for gases and most of the nonmetallic liquids, while equation (5a) is recommended for liquid metals with high h_{in}.

In writing equation (5) it was assumed that the heat radiated from inside of the tube walls from the hot to the cold end is negligible, and that the working fluid is transparent to the internal radiation. Since the flow is considered subsonic, the frictional heating is also ignored. It is also assumed that the inside and outside tube wall temperatures are uniform circumferentially.

Heat-transfer coefficient in turbulent flow: For cooling gases and nonmetallic liquids of moderate viscosity, reference 19 gives the following correlation for heat-transfer coefficient for turbulent flow in long smooth tubes ($Z/D_{in} \geq 60$):

$$h_{in} = 0.023 \frac{k_w}{D_{in}} Re^{0.8} Pr^{0.3} \tag{6a}$$

For cooling liquid metals the following equation is used (ref. 19):

$$h_{in} = 0.625 \frac{k_w}{D_{in}} Re^{0.4} Pr^{0.4} \tag{6b}$$

The properties of the working fluid such as thermal conductivity and viscosity in the Reynolds and Prandtl numbers in equation (6) were evaluated at the arithmetic mean of the fluid inlet and outlet bulk temperatures of the radiator. In case of the liquid or liquid metal fluids, the density and also the specific

heat were determined in the same way. The specific heats of the inert gases were taken as constant and independent of the temperature. For the monatomic gases, the density was computed from the ideal gas law: $\rho = P/RT$.

Presently, there is a scarcity of experimental data for the turbulent-flow heat-transfer coefficients in long smooth tubes with cooling by thermal radiation. Lacking empirical correlations that may be applicable to the space environment conditions, equations (6a) and (6b) for convection heat transfer were chosen because they conveniently allow the use of average bulk temperatures of the fluid. Equation (6a) also accounts, at least partly, for the cooling effect through the Prandtl number raised to the 0.3 power instead of the 0.4 power as it is conventionally used for heating of the fluids.

Heat-transfer coefficient in laminar flow: There is no mathematical solution known to be available to date of the laminar flow in space radiator tubes where the wall temperature varies nonlinearly and wall heat flux varies with the fourth power of the wall temperature. As in turbulent flow, there is also a lack of experimental data for laminar flow being cooled by thermal radiation. Therefore, when the flow is laminar, the following equation for heat transfer by forced convection was used for all three types of the working fluids (liquid metal, liquid, and inert gas):

$$h_{in} = 4.36 \frac{k_w}{D_{in}} \tag{7}$$

Equation (7) arises from a limiting Nusselt number equal to 4.36 for fully developed laminar flow (e.g., ref. 19). This limiting Nusselt number is the same for either constant wall heat flux or linear wall temperature. However, for constant wall heat flux, the thermal-entrance length is one-half the thermal-entrance length for the linear wall temperature (e.g., ref. 19). The thermal-entrance length is that distance from the beginning of the heat transfer at which the Nusselt number becomes independent of the length. If the tubes are not sufficiently long for fully developed laminar flow, the heat-transfer coefficient may be higher than that given by equation (7), and the use of this equation will yield conservative results.

Heat-transfer coefficient in transition region: Heat transfer in turbulent pipe flow is determined by different laws than in laminar flow. Therefore, for the same fluid properties, Reynolds number, and tube diameter, equation (6) will yield different results than equation (7), indicating a sharp discontinuity. In practical applications, however, it can be expected that there is a gradual transition between laminar and turbulent regimes. As the flow in this regime may be very unstable and actual performance may differ considerably from that predicted, there is no generally accepted heat-transfer equation available for the transitional regime. There is also no agreement as to the extent of this region. According to reference 20, by carefully avoiding all disturbances, the Reynolds number for transition may extend from 2300 to 500 000. However, under practical conditions as they prevail in industrial applications, flow in tubes usually is considered turbulent when the Reynolds number exceeds 3000. For the purpose of this report, the flow was considered fully developed laminar up to a Reynolds number of 2300, and fully developed

turbulent when the Reynolds number is equal to or greater than 3000. When the Reynolds number falls between 2300 and 3000, the flow was assumed to be transitional and calculations were made with both sets of equations.

Radiation. - The net heat from the outer surface of a radiator strip is radiated to unobstructed space. Since a flat, symmetrical geometry radiator is considered, the following relation is written for the same equivalent sink temperature on each surface of the radiator

$$(\Delta Q_R)_j = 4\sigma\epsilon R_o N(\Delta z)_j \left(1 + \frac{L}{R_o}\right)\left(T_{o,j}^4 - T_s^4\right)\eta_j \qquad (8)$$

where the fin-tube profile ratio L/R_o and the equivalent sink temperature of space T_s (ref. 16) are independent variables, and the fin-tube effectiveness η_j remains to be defined. If unequal sink temperatures are involved, the individual net emission contributions from each surface have to be treated.

Equivalent sink temperature. - As shown in reference 16, heat influx from the external space environment can be neglected for high-temperature radiators (greater than about 1500° R). For lower temperature radiators, the approximate error involved in neglecting the sink temperature may be considerable. As most of the sensible-heat applications fall in the latter category, the heat influx from the external space environment (space, Sun, and nearby planets) was accounted for in this analysis. The effects of the heat influx were combined in a single quantity called the equivalent sink temperature of space. Although it was treated as an independent variable to simplify the mathematics, the equivalent sink temperature depends on many factors: (1) the vehicle orbit (i.e., circular, elliptical, polar, equatorial), position (sun, shade), and altitude; and (2) the radiator configuration (cylindrical, plane, etc.) and surface properties (emissivity, absorptivity). Details on how to evaluate the equivalent sink temperature of space are given, for example, in reference 16.

Surface emissivity. - Theoretically, when both fins and tubes have nonblack surfaces, as in all practical cases, an extensive computing effort would be required to achieve accurate numerical results for the heat radiated, as demonstrated in reference 21, even if a gray body is assumed. In order to circumvent the analytical difficulties involved, reference 5 presents an approximate method of solution by assuming that the radiator surfaces are isothermal not only axially, but also laterally. An emissivity function $\bar{\epsilon}$, called the apparent emissivity of the central fin-tube cavity, is derived, and it is postulated that the net radiation for a gray body is equal to the net radiation for a blackbody multiplied by the apparent emissivity of the cavity. Presently, there is no known evaluation, however, of how the apparent emissivity method of reference 5 compares with an exact method (e.g., with one outlined in ref. 21). Therefore, for simplicity in this analysis, the blackbody equations for radiation from tubes were modified by arbitrarily including the hemispherical emissivity ϵ as a direct multiplier. A similar approach is used in reference 5 for optimizing condenser-radiators (e.g., eqs. (39) and (40) of ref. 5).

Fin-tube effectiveness. - The fin-tube effectiveness η_j in equation (8)

is evaluated by following the theory of fin-tube effectiveness of condenser-radiators with isothermal base temperature, as discussed in reference 5. The fin-tube effectiveness for an isothermal strip j of the sensible-heat radiator including the effective sink temperature of space is written in a similar way as

$$\eta_j = \frac{1 - \theta_{s,j}^4 + \frac{L}{R_o}\left[\int_0^1 \left(2 - \theta_j^4 - \theta_{s,j}^4\right) F_{\underline{\bar{X}}}\, d\underline{\bar{X}} - \frac{1}{\lambda_j}\left(\frac{d\theta_j}{d\underline{\bar{X}}}\right)_{\underline{\bar{X}}=0}\right]}{\left(1 + \frac{L}{R_o}\right)\left(1 - \theta_{s,j}^4\right)} \tag{9}$$

where λ_j is the conductance parameter, θ is a dimensionless temperature ratio, and $F_{\underline{\bar{X}}}$ is an angle factor, all defined in the following paragraphs.

Equation (9) is based on a dimensionless fin temperature defined as the ratio of local fin surface temperature to local temperature of the base of the fin

$$\theta_j = \frac{T_{\bar{X},j}}{T_{o,j}} \tag{10}$$

where $\underline{\bar{X}}$ is the dimensionless distance from the base surface along the fin width, x/L, as shown in figure 2(b).

The dimensionless sink temperature is defined as the ratio of equivalent sink temperature to local temperature of the base of the fin

$$\theta_{s,j} = \frac{T_s}{T_{o,j}} \tag{11}$$

The conductance parameter λ_j in equation (9) is a dimensionless quantity defined as

$$\lambda_j = \frac{2\sigma\epsilon T_{o,j}^3 L^2}{k_F t} \tag{12}$$

It differs from the blackbody conductance parameter N_c of reference 5 in that the latter does not contain the hemispherical emissivity ϵ so that

$$\lambda = \epsilon N_c$$

Because of the axial temperature gradient, λ for sensible-heat radiators varies along the length of the tube according to

$$\lambda_j = \lambda_1 \left(\frac{T_{o,j}}{T_{o,1}}\right)^3 \tag{13}$$

The angle factor $F_{\underline{\bar{X}}}$ in equation (9) represents the fraction of thermal energy leaving the fin surface at location $\underline{\bar{X}}$, which is incident on adjacent tubes (1 and 2 in fig. 2(b)), or

$$F_{\underline{\bar{X}}} = F_{\underline{\bar{X}}-1} + F_{\underline{\bar{X}}-2} \tag{14}$$

These angle factors are dependent not only on position $\underline{\bar{X}}$ but also on the reciprocal of the fin-tube profile ratio L/R_o. The expression for both angle factors is given, for example, in reference 5.

Equation (9) cannot be solved analytically; therefore, a numerical solution is necessary. The method of solution of equation (9) is given in reference 22. Figure 3 shows the results of this solution, where local fin-tube effectiveness η_j is plotted against local conductance parameter λ_j (eq. (12)) with several local sink temperatures $\theta_{s,j}$ and fin-tube profile ratios L/R_o as parameters.

Résumé

Thus far, heat-transfer considerations alone have provided two basic equations: equation (3) for convection and conduction, and equation (8) for thermal radiation. These equations contain four unknown quantities, namely, incremental length $(\Delta z)_j$, outside tube diameter D_o, number of tubes N, and tube outside temperature $T_{o,j}$. Two more relations are required and these were obtained from the meteoroid protection (appendix B) and pressure drop (appendix C) requirements. Finally, radiator dimensions, panel planform area, and total and component weights were obtained from equations and procedures as outlined in appendixes D to F and as discussed previously in the Approach section.

RADIATOR CHARACTERISTICS

The purpose of this section is first to illustrate the basic thermal characteristics of sensible-heat radiators, such as the variations of the fluid and wall temperatures, the conductance parameter, and the fin-tube effectiveness. It is intended also to show the effect that changes in the geometric parameters, such as tube inside diameter, fin-tube profile ratio, and initial conductance parameter, have on the area and weight as well as other physical characteristics of the radiator. To fulfill the foregoing objectives, three typical sensible-heat radiators for use in space were taken as examples. All calculations for these examples were based on the previous analysis and were obtained from the equations and procedures outlined herein.

The first radiator example illustrates the characteristics of a large heat-rejection unit operating at a high-temperature level with a moderate temperature difference. The temperature level is sufficiently high that a liquid metal is required as the working fluid, and the equivalent sink temperature equal to zero can be used. Such a radiator is typical of one to be used in conjunction with a condenser - heat-exchanger and would serve as the heat rejector, for example, for a 1000-kilowatt electric Rankine cycle power-generating system.

The second radiator example has a small heat-rejection rate, a low-temperature level, and a small temperature drop. The working fluid chosen is

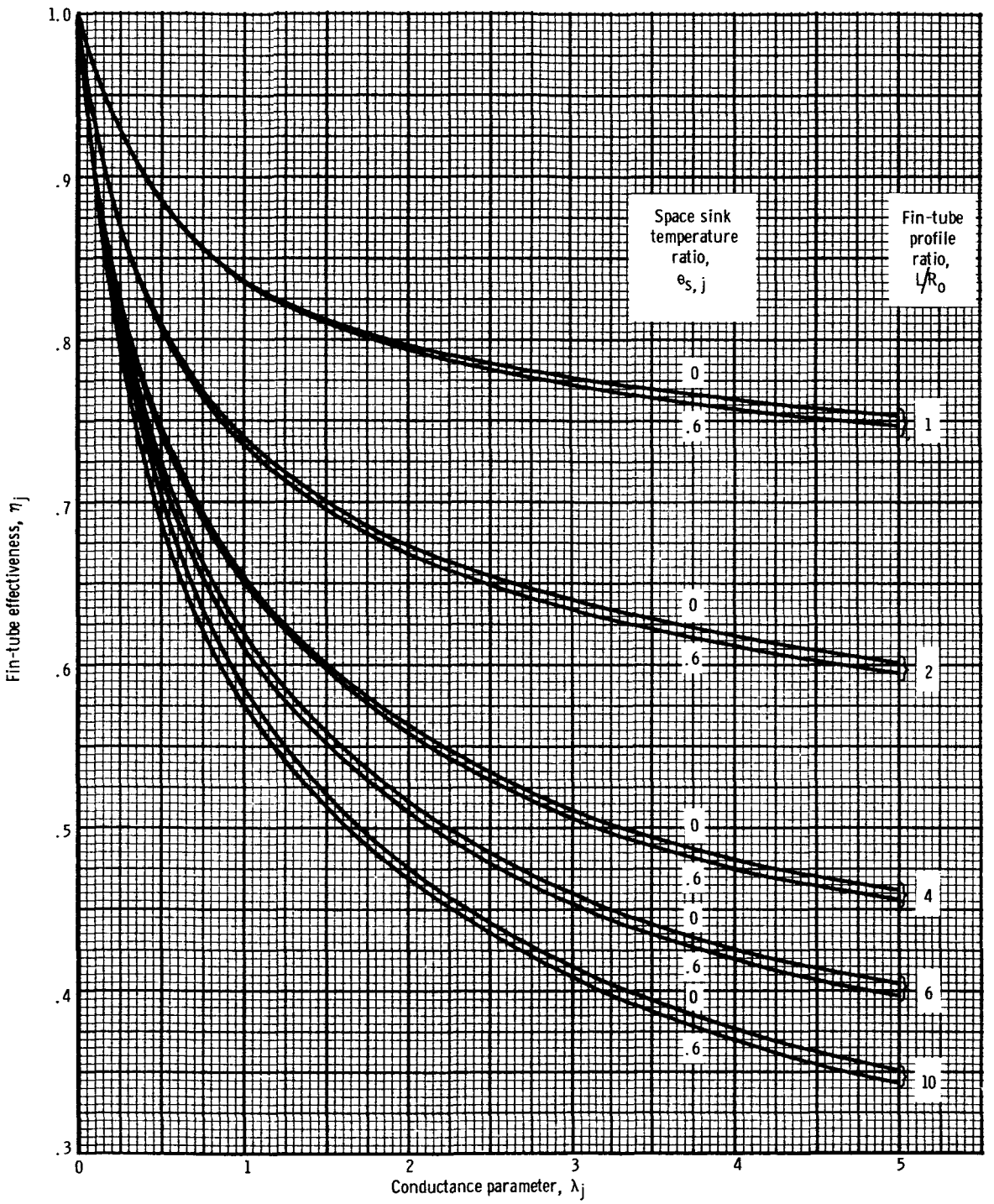

Figure 3. - Fin-tube effectiveness for central-fin-tube flat-plate radiator.

an organic liquid. The temperature level is sufficiently low that the liquid does not decompose, and the pressure required to keep the fluid from vaporization is not excessive. A typical application of this radiator would be for secondary cooling, for example, cooling of seals, bearings, alternator, controls, and pump motors.

The third class can be characterized as radiators with comparatively low heat-rejection rates, moderate temperature level, and large temperature differences. The application is typical of a direct heat-rejection system (gas flow in radiator) to be used in a Brayton cycle that generates several kilowatts of electric power.

The inputs for the computer calculations are obtained from the operating conditions of the three given cycles (Rankine, secondary cooling, or Brayton); from selected tube, fin, header, and liner materials; and from meteoroid protection and environment requirements. In addition, there is a choice of several independent parametric variables. The specific inputs required to obtain the results for the particular three examples described are given in table I. Inputs listed in table I(a) to (c) were kept constant, while profile ratios, tube inside diameters, and initial conductance parameters (table I(d)) were varied one at a time over the ranges indicated in the table. Thus, a series of outputs was generated that was used to describe the radiator thermal and physical characteristics.

The radiator thermal properties include the axial and radial temperature variations and axial changes of conductance parameter. This class of outputs is augmented by axial variations that occur in fin-tube effectiveness and the fraction of heat radiated from the fins. These results for radiators that have weights near minimum are presented first.

The outputs describing radiator physical characteristics are discussed next. It will be shown how the parametric variations of tube inside diameter, fin-tube profile ratio, and initial conductance parameter affect the total radiator weight, planform area, component weights, number and length of tubes, length, width, and thickness of the fins, and header length and inside diameters.

After the thermal and physical characteristics of the three radiators have been presented, they are compared in the closing portion of this section. Any radiator characteristics that might be attributable to a particular range of heat-rejection rate, temperature level, temperature difference, or class of working fluid will also be indicated.

Rankine Cycle Radiator

A schematic diagram of the arrangement in which a sensible-heat radiator may be used in conjunction with a condenser - heat-exchanger as the heat-rejection system for a Rankine cycle is shown in figure 4(a). Wet vapor of the cycle working fluid enters one side of the condenser from the turbine and leaves as a subcooled liquid. A pump is used to circulate the cycle working fluid as would be the case in a Rankine cycle with a condenser-radiator

TABLE I. - CALCULATION INPUTS

(a) Operating conditions

Inputs			Class of radiators		
Name	Symbols	Units	Rankine	Secondary cooling	Brayton
Heat-rejection rate	Q_R	Btu/sec	4367	20	28.3
Working fluid	-----	-------	NaK	Ether (ET-378)	Argon
Flow rate	$\dot{m}$	lb/sec	138.83	1.4245	0.53
Specific heat	c_p	Btu/(lb)(^oR)	0.2097	0.39	0.124
Viscosity	μ	lb/(ft)(sec)	0.1111×10^{-3}	0.365×10^{-2}	0.196×10^{-4}
Thermal conductivity	k_w	Btu/(sec)(ft)(^oR)	0.4144×10^{-2}	0.226×10^{-4}	0.37×10^{-5}
Gas constant	R	ft-lb/(lb)(^oR)	----------	----------	38.7
Fluid density	ρ_L	lb/cu ft	45	69.5	----------
Inlet temperature	T_i	^oR	1700	706	967
Exit temperature	T_f	^oR	1550	670	536
Inlet pressure	P_i	lb/sq ft	----------	----------	950
Tube-pressure-drop ratio	$\left(\frac{\Delta P}{P_i}\right)_t$	----------	----------	----------	0.064
Header-pressure-drop ratio	$\left(\frac{\Delta P}{P_i}\right)_H$	----------	----------	----------	0.008
Tube pressure drop	$(\Delta P)_t$	lb/sq ft	432	1440	----------
Header pressure drop	$(\Delta P)_H$	lb/sq ft	72	288	----------

(b) Selected material properties

Material (fins and armor)	-----	----------	Beryllium	Aluminum	Aluminum
Material (liner)	-----	----------	Columbium alloy	----------	----------
Sonic velocity in armor material	c	ft/sec	35 700	16 600	16 400
Fin density	ρ_F	lb/cu ft	115	169	169
Header density	ρ_H	lb/cu ft	115	169	169
Tube density	ρ_t	lb/cu ft	115	169	169
Liner density	ρ_c	lb/cu ft	530	----------	----------
Fin thermal conductivity	k_F	Btu/(hr)(ft)(^oR)	54	110	111
Surface emissivity	ϵ	----------	0.9	0.9	0.9

(c) Meteoroid protection and environment

Probability of no penetration	P(0)	----------	0.995	0.9	0.9
Operation time	τ	days	500	365	365
Occlusion factor	$\overline{C}$	----------	1	1	1
Meteoroid density	ρ_P	g/cu cm	0.44	0.44	0.44
Average meteoroid velocity	$\overline{V}$	ft/sec	98 400	98 400	98 400
Meteoroid mass distribution constant	α	$gm^\beta/(sq\ ft)(day)$	0.53×10^{-10}	0.53×10^{-10}	0.53×10^{-10}
	β	----------	1.34	1.34	1.34
Spalling factor	a	----------	1.75	1.75	1.75
Sink temperature	T_s	^oR	0	400	400

(d) Parametric variables

Tube inside diameter	D_{in}	in.	0.375 - 1.00	0.0625 - 0.50	0.750 - 1.50
Liner thickness in tubes and headers[a]	δ_c	in.	0.04 D_{in}	----------	----------
Fin-tube profile ratio	L/R_o	----------	1 - 4	6 - 16	2 - 10
Initial conductance parameter	λ_1	----------	0.2 - 1.5	0.2 - 1.0	0.2 - 2.0

[a]Not less than 0.015-in.

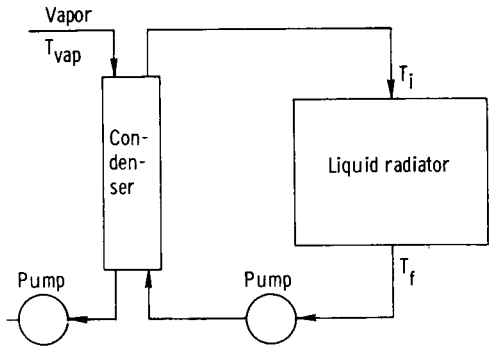

(a) Schematic diagram.

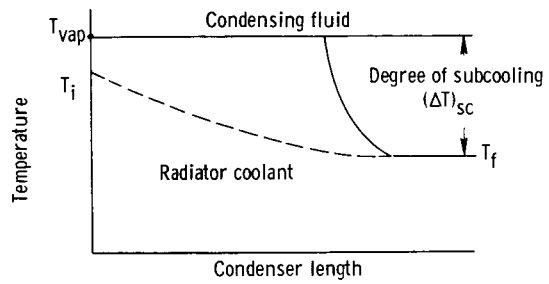

(b) Temperature diagram.

Figure 4. - Diagrams for sensible-heat radiator with condenser - heat exchanger used in Rankine cycle.

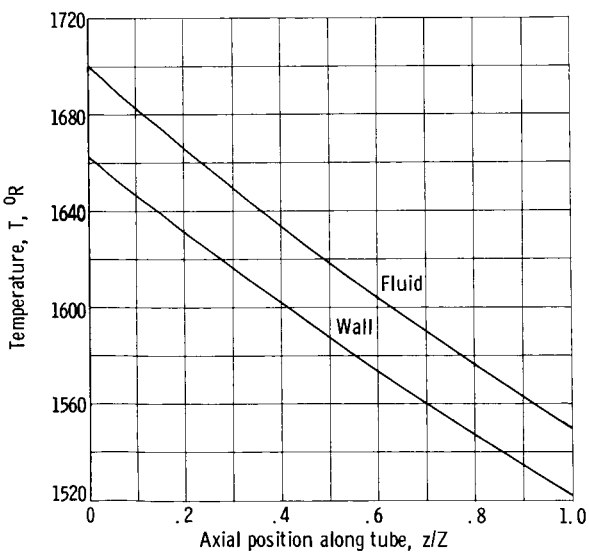

Figure 5. - Variations of fluid and wall temperatures with tube length for Rankine cycle radiator example. Power level, 1000 kilowatts. (See table I for operating conditions.)

(ref. 5). Liquid metal from the radiator is pumped through the other side of the heat exchanger where it absorbs the heat of condensation of the working fluid as well as the sensible heat corresponding to the subcooling of the working fluid.

The temperatures on both sides of the heat exchanger are illustrated as a function of condenser length in figure 4(b) for a counterflow arrangement. For simplicity, it was assumed that the cycle working fluid maintains the saturation temperature corresponding to the pressure at the turbine exhaust until the working fluid is completely condensed. Its temperature then falls rapidly to the final temperature of the subcooled working fluid. Because of the high heat-transfer coefficients on both sides of the condenser - heat-exchanger, the heat-exchanger exit temperature of a Rankine cycle working fluid is almost equal to the temperature of the coolant entering the heat exchanger from the radiator. This means that the final subcooled temperature of the working fluid $T_{vap} - \Delta T_{sc}$ is determined by the temperature of the coolant leaving the radiator T_f (fig. 4(b)). The thermodynamics of the heat exchanger are such that the temperature of the coolant coming out, which is the same as the inlet temperature to the radiator T_i, can be no higher than the saturated vapor temperature of the working fluid T_{vap}.

The example chosen to illustrate the thermal and physical properties of such a radiator employs a sodium-potassium alloy (NaK-78) as the heat-transfer medium. The heat-rejection rate is 4367 Btu per second, typical of a 1000-kilowatt Rankine cycle powerplant (ref. 5). The physical and thermal properties of NaK were used as given in reference 23. The tube and the header inner liners were made of a columbium alloy, and the tube and the header armor

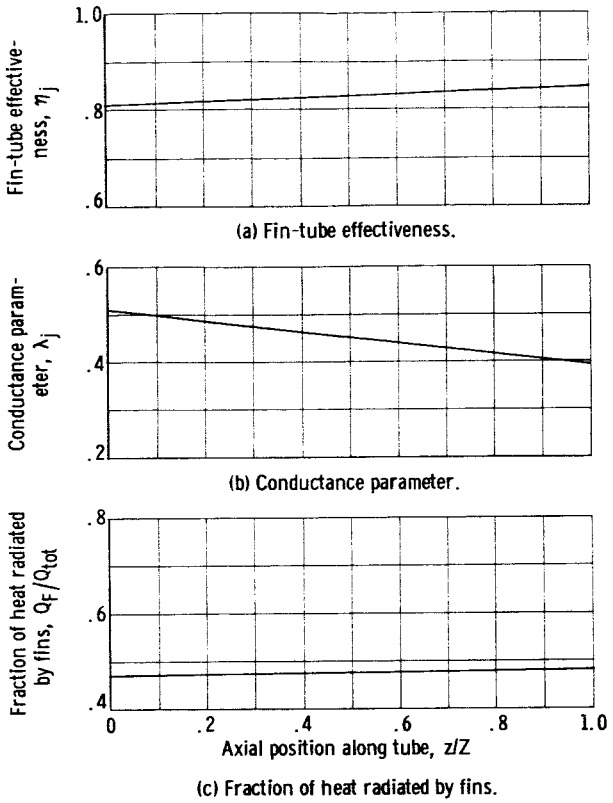

Figure 6. - Thermal characteristics of Rankine cycle radiator example. Power level, 1000 kilowatts. (See table I for operating conditions.)

and fins were made of beryllium. Over the range of independent parametric variables investigated (see table I, p. 15), the flow of NaK was entirely in the turbulent region.

Thermal characteristics. - The example studied has a 0.625-inch tube inside diameter, an initial conductance parameter equal to 0.5, and a fin-tube profile ratio of 2. Parametrically these values were shown to correspond to a radiator with a total weight near the minimum point for the inputs considered.

Temperature variations of the liquid-metal NaK and beryllium tube outside wall are shown in figure 5. Both temperature curves are nearly linear because of the relatively small temperature difference between tube inlet and exit. It indicates almost a constant heat-rejection rate per unit length of the radiator. The small radial temperature drop between the fluid and the wall is characteristic of liquid metals with good heat-transfer properties.

The level of fin-tube effectiveness η_j for this example, as shown in figure 6, is high. As the temperature variation along the tube length is small, the effectiveness curve is nearly linear. The curve of conductance parameter λ_j plotted in the same figure, shows a similar linear behavior along the tube length. The fin heat-rejection rate is also shown in figure 6 as a fraction of the total radiator heat-rejection rate: the fraction is relatively small. Nowhere does the fin heat-rejection fraction exceed 50 percent of the total heat-rejection rate.

Physical characteristics. - Since the computer program does not have a minimization procedure for radiator total weight, the minimum weights were determined graphically. The graphical minimization of the total weight for a 0.625-inch tube inside diameter is illustrated as an example in figure 7.

The fact that values of initial conductance parameter and fin-tube profile ratio need not be precisely defined in order to achieve near minimum radiator weight is more explicitly shown for the same fixed tube diameter in figure 8. Zones of minimum weight plus 1 percent and plus 1/2 percent indicate a wide range of permissible profile ratios and initial conductance parameters for this example.

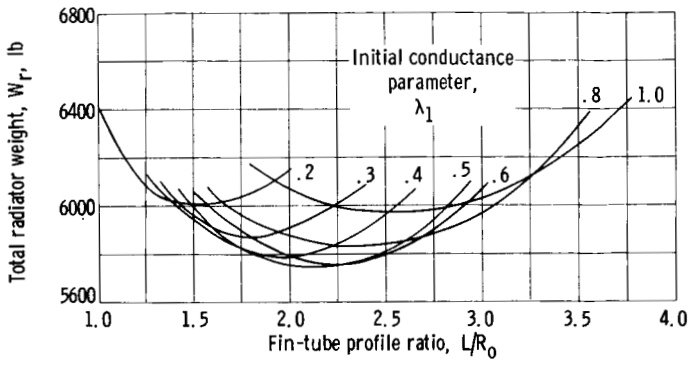

Figure 7. - Variations of total weight with fin-tube profile ratio and initial conductance parameter for Rankine cycle radiator example. Tube inside diameter, 0.625 inch; power level, 1000 kilowatts. (See table I for operating conditions.)

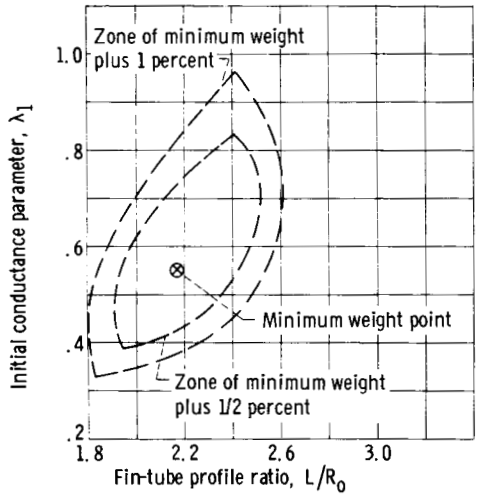

Figure 8. - Zones of profile ratios and initial conductance parameters for near-minimum weights of Rankine cycle radiator example. Power level 1000 kilowatts; tube inside diameter, 0.625 inch. (See table I for operating conditions.)

In a similar way, the minimum weights were obtained for other tube inside diameters. The resulting total and component weights and corresponding panel planform areas are plotted against tube inside diameter in figures 9(a) and (b). It is seen that total minimum weight occurs at a tube inside diameter slightly less than 0.625 inch. Since the latter may be a readily available tube size, it has been selected to represent the "minimum weight" tube size in the subsequent discussions. The changes in the panel planform area (fig. 9(b)) over the range of tube diameters shown are linear with tube inside diameter and follow the slope of the fin weight curve (fig. 9(a)).

It is also seen from figure 9(a) that more than 50 percent of the total minimum weight is contributed by the tube weight. The main contributor to the tube weight is tube armor, since liner weight is a very small part of the tube weight. The heavy armor weight in this example is a result of the severe protection requirements of very high probability of no meteoroid penetration, long operation time, and no redundancy (single panel) as indicated in table I (p. 15). The remainder of the weight at the minimum weight diameter (0.625 in.) is nearly equally divided among headers, fins, and liquid content weight.

The tube inside diameter for minimum weight is a function of the interplay of several factors. In this example, the header and liquid content weights decrease, and tube and fin weights increase as the tubes are enlarged. As a result of these opposing trends in component weights, the total radiator weight first decreases, passes through a minimum value, and then increases as the tube inside diameter increases. Thus, the headers and liquid content, being a relatively large percentage of total weight, give a large optimum tube inside diameter. Different design inputs (e.g., pressure drop in headers or tubes) may change the proportions of the individual component weights, and as a consequence, also change the magnitude of the tube inside diameter at which the radiator total minimum weight occurs.

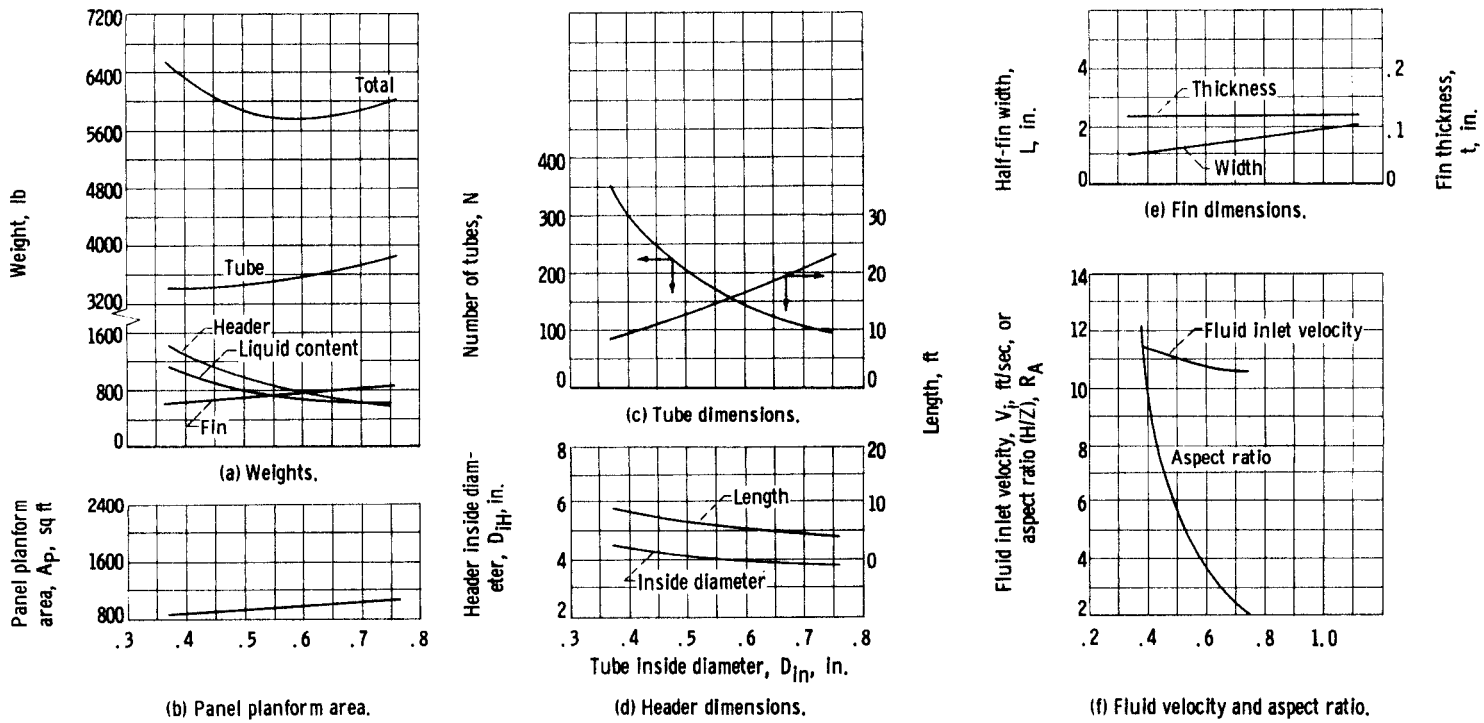

Figure 9. - Variations of physical characteristics with tube inside diameter for Rankine cycle radiator example. Power level, 1000 kilowatts. (See table I for operating conditions.)

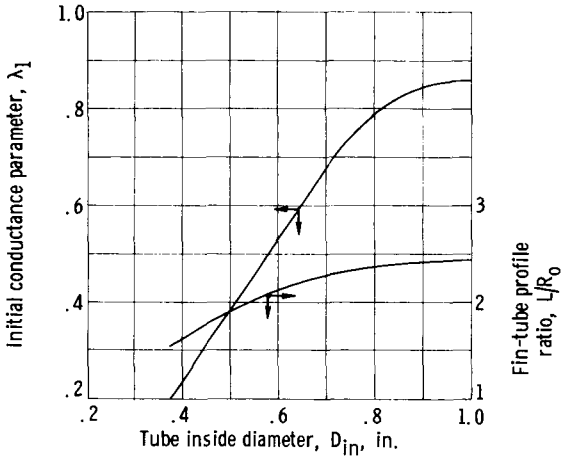

Figure 10. - Variations of initial conductance parameter and fin-tube profile ratio with tube inside diameters at minimum weights for Rankine cycle radiator example. Power level, 1000 kilowatts. (See table I for operating conditions.)

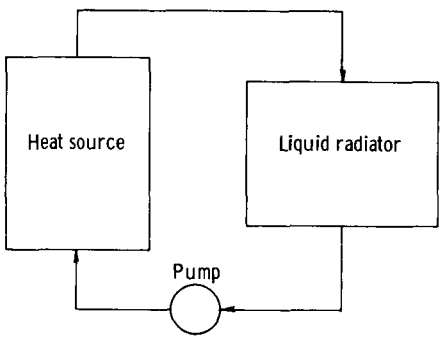

Figure 11. - Schematic drawing of secondary cooling radiator.

A better understanding of various weight curves can be obtained from figures 9(c) to (e), where the quantities that describe the radiator geometry are plotted against the tube inside diameter. It is seen that, for small tube diameters, there are a large number of short tubes that yield long and heavy headers with large inside diameters. Therefore, the aspect ratio tends to be high, as shown in figure 9(f). As the diameters are increased, the number of tubes becomes smaller and the tubes longer. As a result, the header length, diameter, and, consequently, the header weight, as well as aspect ratio decrease. The aspect ratio can also be controlled, if the pressure drop in the tubes can be varied independently. As can be shown by combining equations (D7), (D12), and (D13), the aspect ratio can be decreased if the allowable tube pressure drop is increased. Figure 9(f) also shows the variations in fluid velocity at the tube inlet to be relatively small.

Figure 10 shows the profile ratios and conductance parameters corresponding to minimum weight at each diameter for the range of tube inside diameters investigated. These values were derived from curves similar to those shown in figure 7 for each tube diameter. Figure 10 indicates that, in general, for the Rankine cycle radiator used as an example, both L/R_o and λ_1 increase with an increase in tube size. It should be emphasized that for each tube diameter there is a considerable choice of either L/R_o or λ_1 without a significant departure from minimum weight. For this particular example, the freedom of choice in L/R_o and λ_1 for a given percentage increase above minimum weight tended to enlarge as the tube diameter increased. The scope of this flexibility has been illustrated in figure 8 for the 0.625-inch diameter.

Secondary Cooling Radiator

A typical application of the radiator illustrated by this example is for secondary cooling, as shown schematically in figure 11. In this figure, the components to be cooled are identified as the heat source. Secondary cooling radiators usually have low heat-rejection rates with small axial temperature differences. The temperature level is also comparatively low. The working

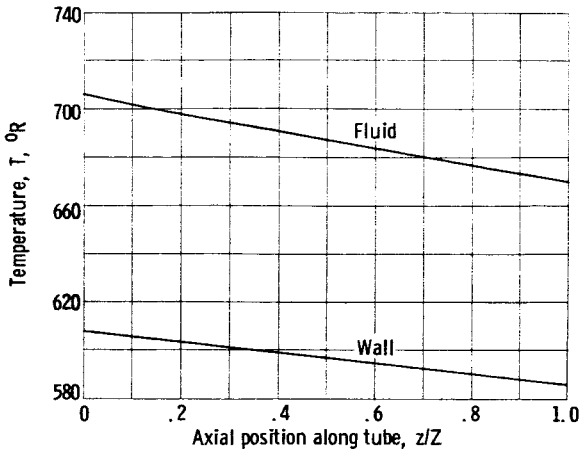

Figure 12. - Variations of fluid and wall temperatures with tube length for secondary cooling radiator example. Heat-rejection rate, 20 Btu per second. (See table I for operating conditions.)

fluid is generally a hydraulic liquid, which may be selected not only for its heat-transfer properties but, in some cases, for its lubrication capabilities. For this example, hydraulic liquid (ether ET-378, ref. 24) was used as a working fluid because of its lubrication qualities. It has been considered for the secondary cooling and lubrication loop in the SNAP-8 system (information received from Aerojet/General Corp.). The heat-rejection rate, 20 Btu per second, was also chosen approximately the same as for the SNAP-8 secondary radiator.

Both laminar and turbulent flows were investigated. The results indicated that, at lower tube inside diameters, the flow was fully developed laminar; however, at larger diameters laminar, turbulent, or mixed flow may be present as indicated by the Reynolds number. For the purpose of this report, the flow was assumed to be uncertain when the Reynolds number fell between 2300 and 3000. The calculations in this region were therefore made by using both sets of equations (laminar and turbulent). Although performance of the radiator in this flow region cannot be predicted with certainty, the results may be of some interest.

Thermal characteristics. - Much that was said about Rankine cycle radiators with NaK as the working fluid can be applied directly to secondary cooling radiators. But there are also some major differences. These will be discussed for a secondary cooling radiator having a 0.125-inch tube inside diameter, an initial conductance parameter of 0.5, and a fin-tube profile ratio of 12. These values correspond to a near minimum weight radiator for the inputs considered (table I, p. 15).

As shown in figure 12, the axial fluid and tube wall temperatures are linear between the inlet and the exit for the secondary cooling radiator employing ether because the working fluid temperature differences are small. There are, however, large radial temperature differences between the liquid and the tube wall, a result of the relatively poor heat-transfer properties of the ether. The poor heat-transfer characteristics were accepted because, in this example, the liquid is used also as a lubricant. In general, less viscous liquids will yield higher heat-transfer coefficients, and, consequently, if such fluids are used in secondary cooling radiators, smaller radial temperature differences (and, consequently, smaller surface area) can be expected.

As expected, conductance parameters, fin-tube effectiveness, and fin heat-rejection rates are nearly linear with axial position, as shown in figure 13, and the magnitudes of all these variations are quite small. The fin-tube effectiveness is somewhat lower than that for the Rankine cycle radiator example. On the other hand, the fraction of heat radiated by the fins for the secondary cooling radiator example is quite high, much higher than that for the

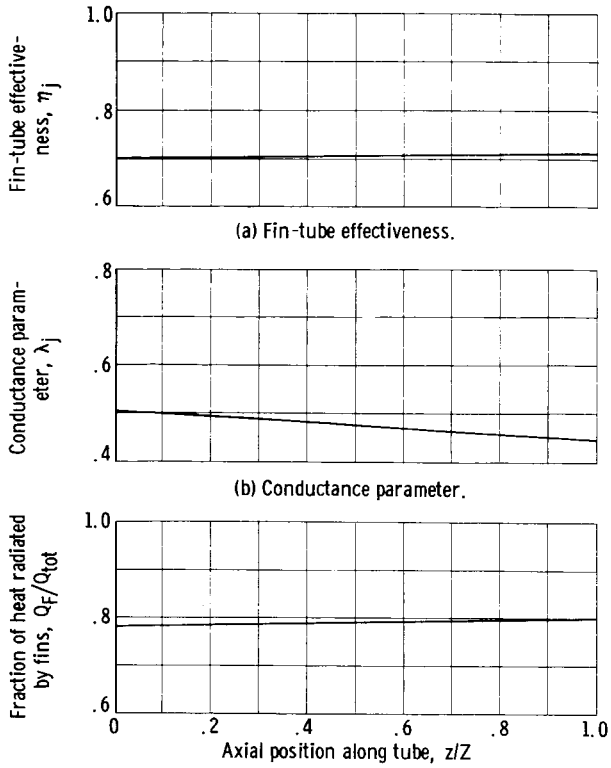

(a) Fin-tube effectiveness.

(b) Conductance parameter.

(c) Fraction of heat radiated by fins.

Figure 13. - Thermal characteristics of secondary cooling radiator example. Heat-rejection rate, 20 Btu per second. (See table I for operating conditions.)

Rankine cycle radiator example because of the smaller tube inside diameter and the larger fin-tube profile ratio.

There are considerable viscosity changes with temperature for most viscous liquids. When the temperature is decreased, the viscosity increases, sometimes by several orders of magnitude; however, the analysis developed in this report is valid only for cases of moderate viscosity changes where the effect of these variations on heat-transfer coefficients and friction factors can be neglected. In this particular example, the viscosity changes are relatively small because of the small temperature range as specified by the required operating conditions. For radiators where large temperature variations and viscous fluids are required, a new analysis may be needed that considers the variations of viscosity and its effect on heat transfer and pressure drop. In some cases, however, the analysis covered by this report still may be useful. By comparing the two results, one with the viscosity corresponding to the liquid inlet temperature and the other with the viscosity determined at the liquid outlet temperature, it is possible to assess the limits of radiator physical characteristics within which an actual radiator design may lie.

Physical characteristics. - Minimum weights for each tube inside diameter were obtained for the secondary cooling radiator example by the same method described previously for the Rankine cycle radiator example; that is, the minimum weights for each tube inside diameter were obtained graphically by enveloping a series of initial conductance parameter curves (as in fig. 7, p. 18). These minimum radiator weights with their component weights and panel planform areas are shown in figures 14(a) and (b) as functions of the corresponding tube inside diameters. As in the Rankine cycle radiator example, the decreasing header and liquid content weights added to increasing tube and fin weight create a minimum in total weights. Contrary to the previous example, the header and liquid content weights for the secondary cooling radiator are a relatively smaller percentage of the total radiator weight. Therefore, the minimum weight occurs at a smaller tube diameter (0.125 in.).

The liquid content curve shows a trend that may be true for all radiators that use liquid or liquid metal as a working fluid. For small tube diameters, the header inside volume is large compared with the volume inside the tubes, and the curve for liquid content weight follows the header weight curve. As

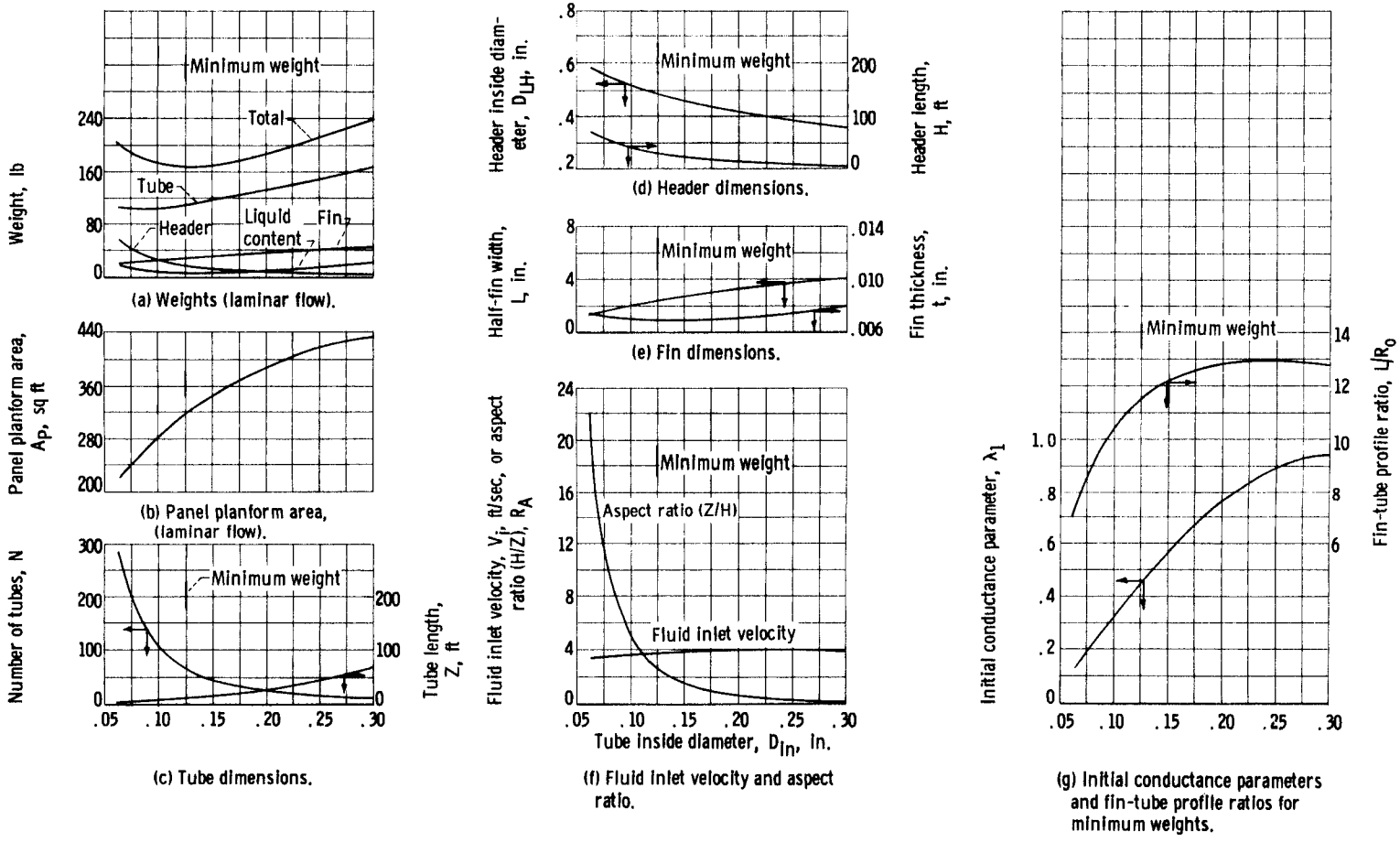

Figure 14. - Variations of physical characteristics with tube inside diameters for secondary cooling radiator example. Heat-rejection rate, 20 Btu per second. Laminar flow. (See table I for operating conditions.)

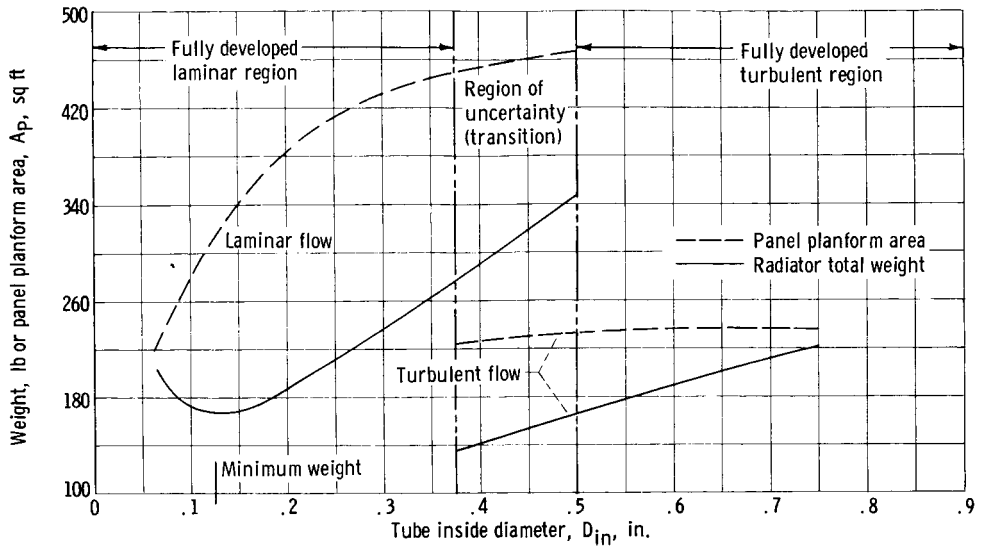

Figure 15. - Comparison of radiator total weights and panel planform areas for laminar and turbulent flows with tube inside diameter for secondary cooling radiator example. Heat-rejection rate, 20 Btu per second. (See table I for operating conditions.)

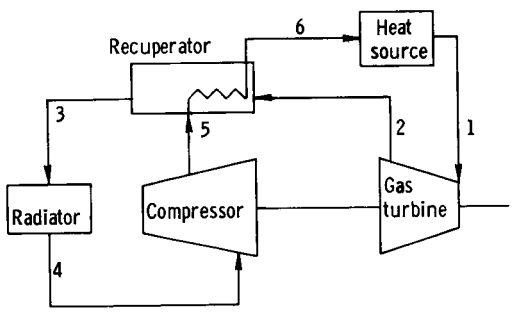

(a) Schematic diagram.

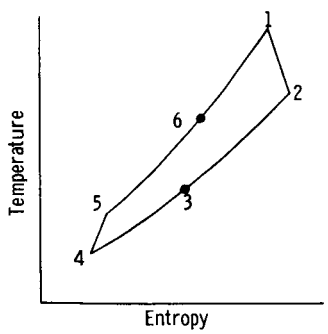

(b) Thermodynamic diagram.

Figure 16. - Brayton cycle diagrams.

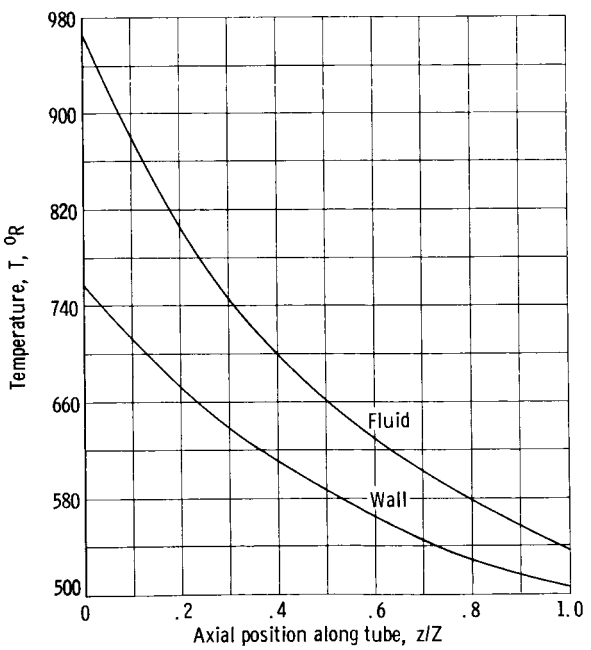

Figure 17. - Variations of fluid and wall temperatures with tube length for Brayton cycle radiator example. Power level, 8 kilowatts. (See table I for operating conditions.)

the tube inside diameters increase, the header volume decreases, and the curve for liquid content weight tends to follow the tube weight curve.

The quantities that describe radiator and header geometry for laminar flow conditions are plotted against tube inside diameter in figure 14(c) to (e) (p. 23). Fluid inlet velocity and aspect ratio are shown in figure 14(f). The same general trends prevail with tube inside diameter for the secondary cooling radiator example as for the Rankine cycle radiator example. Figure 14(g) shows fin-tube profile ratios and initial fin conductance parameters for minimum weight for each tube inside diameter. As indicated previously, however, large departures from these values can be tolerated with a very small increase in radiator weight.

Figure 15 (p. 24) compares the total weights and panel planform areas obtained from the laminar flow equations with those obtained from the turbulent flow equations. It is seen that weight and area can be considerably reduced if, at larger tube diameters, early transition to fully developed turbulent flow can be promoted.

Brayton Cycle Radiator

The radiator used for this example typically performs the service required from the heat-rejection unit in a Brayton cycle power system shown schematically in figure 16. The system generates several kilowatts of electricity. The heat-rejection rate is 28.3 Btu per second, and the working fluid is argon. The physical and thermal properties of argon are taken from reference 25. For all cases investigated for this example, the flow was fully turbulent.

Thermal characteristics. - The gas temperature variations, along with the temperature of the wall, are shown in figure 17. The example selected had a 1-inch tube diameter, a fin-tube profile ratio of 6, and an initial conductance parameter of 1. For both temperature curves, the slope has the largest negative value at the tube inlet. The heat-rejection rate, being related to the fourth power of the wall temperature, is greatest at the tube inlet and accounts for the rapid decrease of temperature in this region. The large temperature difference between the wall and the gas is evidence of the relatively low convective heat-transfer coefficient of the gas. In the analysis, it was assumed that the convective heat-transfer coefficient between the gas and the wall was constant over the entire tube length. As a result, with the heat-rejection rate decreasing as the gas proceeds along the tube, the temperature difference between the fluid and the wall also decreases (eq. (3)).

Figure 18 shows the changes in the conductance parameter, fin-tube effectiveness, and fraction of heat radiated by the fins as a function of axial position along the tube length. It is seen that the principal characteristics of these parameters are large decreases of conductance parameter along the tube length (by ~70 percent) and the large amount of heat rejected by the fins (~75 percent).

Physical characteristics. - In order to generate the minimum weight envelope curve for the Brayton cycle radiator, which has relatively few tubes, a

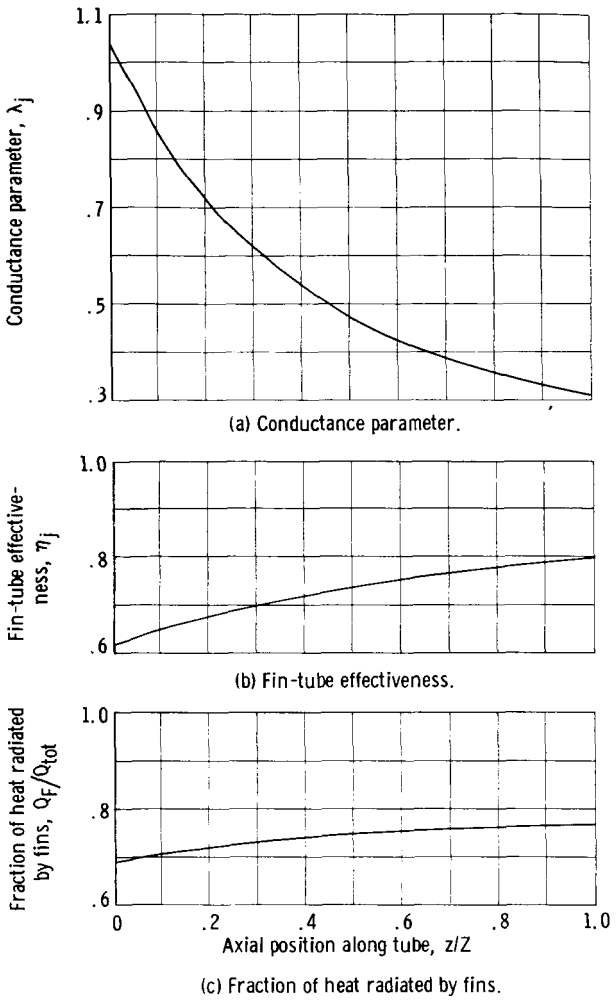

Figure 18. - Thermal characteristics of Brayton cycle radiator example. Power level, 8 kilowatts. (See table I for operating conditions.)

more elaborate procedure had to be employed than that used for the Rankine and secondary cooling radiator examples. The method is discussed in appendix G. The minimum weight thus obtained for each tube inside diameter is shown in figure 19(a). Since the fluid content weight for inert gases is very small, it is not shown. As in the previous example, the decreasing header weights are opposing the increasing tube and fin weights, thus creating a minimum in combined weights at about a 1.00-inch tube inside diameter. The headers again are relatively heavy so that minimum weight occurs at a large diameter. Compared with the Rankine cycle and secondary cooling radiator examples, the total minimum weight of the Brayton cycle radiator is less sensitive to diameter changes over a wider range. The effect of tube diameters on panel planform area is also small for the values of diameter covered.

Figures 19(c) to (e) shows some further quantities that describe the radiator and headers as functions of the tube inside diameter. As the diameter increases, the tube length, fin width, and fin thickness (after undergoing a slight decrease) increase. For the smaller tube diameters, the combination of a large number of shorter tubes leads to a radiator panel with a large aspect ratio, as shown in figure 19(f). The same figure also illustrates the velocities at the tube inlet as a function of tube inside diameter. The velocities are small compared with their sonic velocities, and the effect of turning losses at tube-header junctions is expected to be small.

Figure 20 shows the fin-tube profile ratio and the initial conductance parameters corresponding to minimum total weights for each tube inside diameter. The initial conductance parameter varies substantially with tube inside diameter, but the fin-tube profile ratio is essentially constant. As in previous examples, wide choices of L/R_o and λ_1 are available to maintain a near minimum weight design.

Comparison of Characteristics

The three examples considered in the previous sections covered a wide

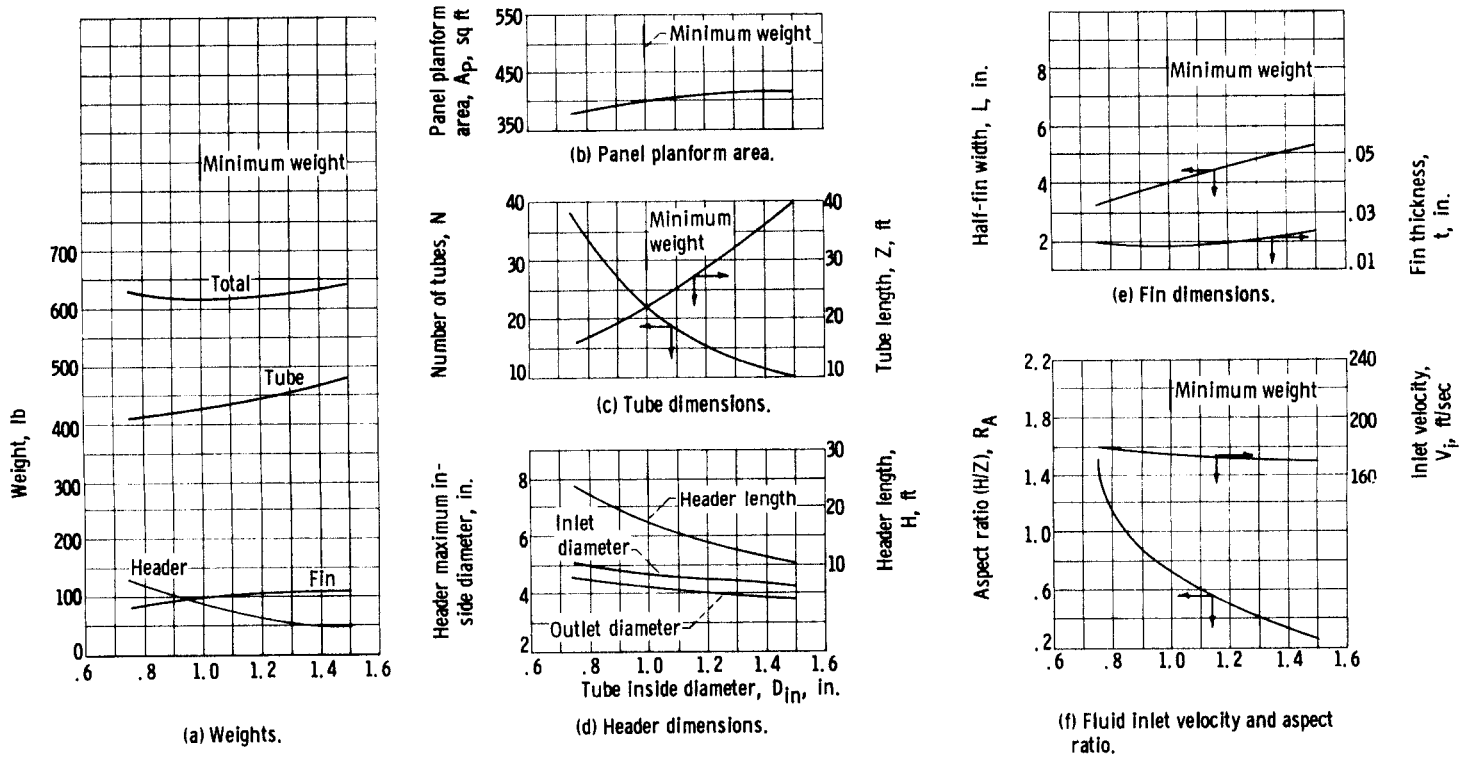

Figure 19. - Variations of physical characteristics with tube inside diameter for Brayton cycle radiator example. Power level, 8 kilowatts. (See table I for operating conditions.)

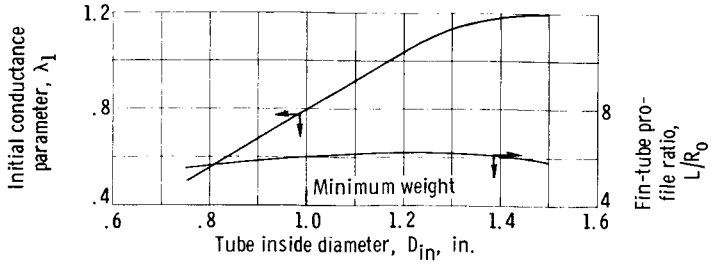

Figure 20. - Variations of initial conductance parameter and fin-tube profile ratio for minimum weights with inside diameters for Brayton cycle radiator example. Power level, 8 kilowatts. (See table I for operating conditions.)

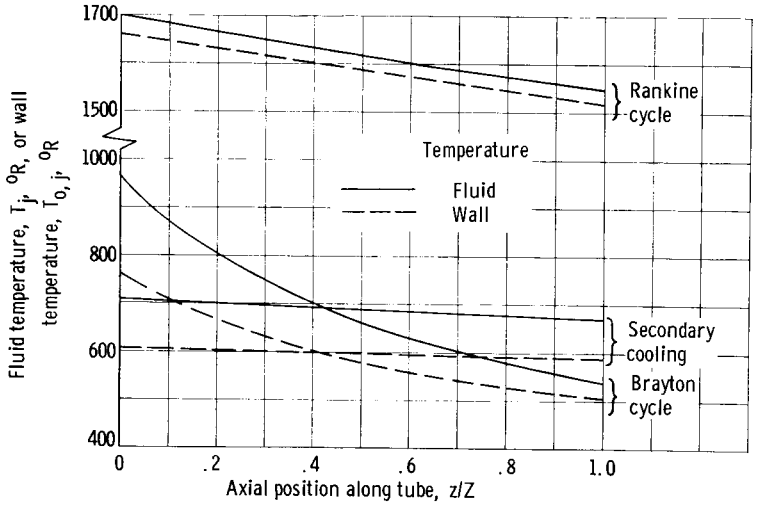

Figure 21. - Comparison of fluid and wall temperatures of three radiator examples.

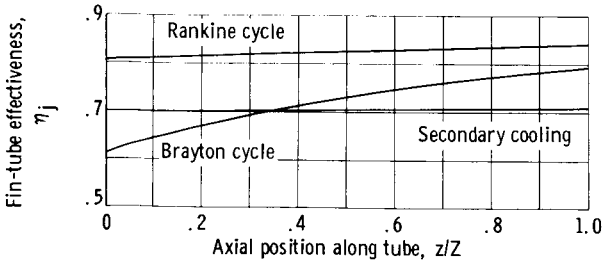

Figure 22. - Comparison of fin-tube effectiveness of three radiator examples.

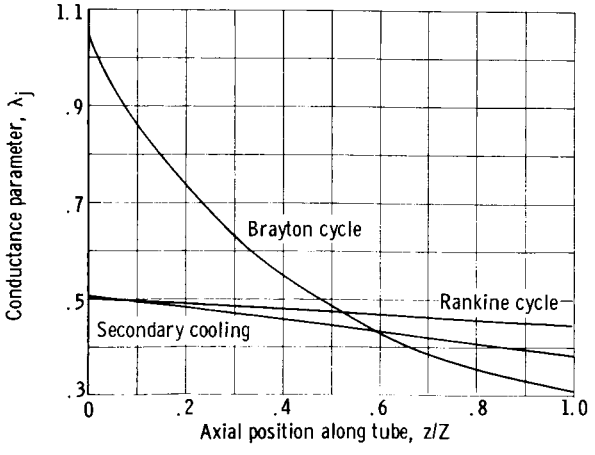

Figure 23. - Comparison of conductance parameter of three radiator examples.

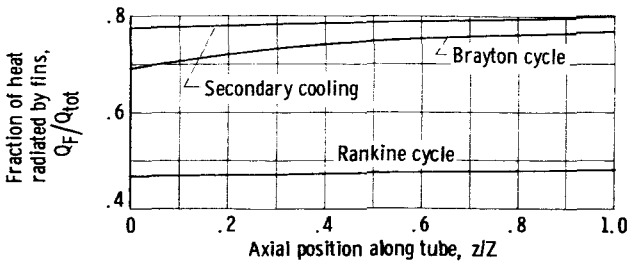

Figure 24. - Comparison of fraction of heat radiated by fins for three radiator examples.

range of radiator heat-rejection rates. Corresponding to these heat-rejection rates, the maximum temperatures of the working fluids ranged from about 700° to 1700° R. Consequently, each type of these sensible-heat radiators exhibited different thermal and physical characteristics. Although the results for the examples considered may not necessarily be precisely representative for all radiators in each class considered, a comparison of the resultant characteristics of the examples may nevertheless prove to be of interest.

Thermal characteristics. - Sensible-heat thermal radiators are distinguished for their axial variations not only of the fluid and tube wall temperatures (fig. 21) but also of fin-tube effectiveness, conductance parameters, and the fraction of heat radiated from the fins. Therefore, the magnitude of the longitudinal temperature difference determines the profile of the properties that are temperature dependent. Comparisons of these thermal characteristics for near minimum weight radiators in each class are given in figures 21 to 24.

When the temperature difference is relatively small and the tube length relatively large, as in the secondary cooling and the Rankine cycle radiator examples, temperature, effectiveness, conductance parameter, and fin heat-rejection ratios tend to approach a straight-line relation with the tube length. When the axial temperature difference is large, as in the Brayton cycle radiator example, the temperature variations are no longer linear with heat-rejection rate but are greatest at the tube inlet.

Large axial temperature variations give rise also to large variations in fin-tube effectiveness (fig. 22) and conductance parameter (fig. 23). The fin heat-rejection ratio is less affected by axial temperature difference (fig. 24). The level of this ratio depends mainly on L/R_o. The secondary cooling radiator example has the highest fin-tube profile and fin heat-rejection ratio; the Rankine cycle radiator example has the lowest.

In the comparison of fluid and wall temperatures shown in figure 21, the temperature difference is a function of the convective heat-transfer coefficient as well as the local heat-rejection rate; when the local heat-rejection rate varies appreciably with tube length, as in the Brayton cycle radiator example, the radial temperature difference also varies appreciably. On the other hand, with heat-rejection rates for the Rankine cycle and secondary cooling radiator examples nearly constant, the wall temperatures almost parallel the fluid temperatures. Argon and ether had the poorest heat-transfer properties of the three examples, and they experienced the largest radial temperature drops. As NaK is a much better heat-transfer fluid, it had relatively smaller radial temperature differences.

Minimum weight radiators. - The principal characteristics of the three radiators at minimum weight are given in table II.

TABLE II. - CHARACTERISTICS OF MINIMUM WEIGHT RADIATORS

Parameters	Symbols	Units	Radiator example		
			Rankine cycle	Secondary cooling (laminar flow)	Brayton cycle
Heat-rejection rate	Q_R	Btu/sec	4367	20	28.3
Total weight	W_r	lb	5772	167	615
Fin-tube profile ratio	L/R_o	-------	2.17	11.5	5.6
Initial conductance parameter	λ_1	-------	0.55	0.45	0.8
Aspect ratio (H/Z)	A_R	-------	3.27	2.48	0.71
Reynolds number	Re	-------	228 000	745	18 780
Fluid inlet velocity	V_i	ft/sec	10.8	3.75	174
Panel planform area	A_P	sq ft	993	317	393
Number of tubes	N	-------	134	64	22
Single tube length	Z	ft	17.4	11.3	23.5
Inside tube diameter	D_{in}	in.	0.625	0.125	1.0
Half-fin width	L	in.	1.76	2.45	3.88
Fin thickness	t	in.	0.121	0.007	0.018

Comparison of the three examples shows that each had a unique set of geometric parameters: fin-tube profile ratio, fin conductance parameter at the radiator entrance, and tube inside diameter for a minimum weight radiator. As mentioned earlier, the minimum weights were determined graphically, and therefore they may not necessarily represent precisely the actual values.

There are several factors responsible for the fact that the minimum weight occurred at the particular values listed in table II (e.g., magnitudes of heat-rejection rates, mass flow rates, temperature level, pressure level and allowable pressure drop, and radiator materials). Therefore, it may not be possible analytically to predict a set of desired parameters beforehand that will automatically, without further parametric studies, yield the minimum weight radiators.

For the examples compared in table II, the absolute minimum weight of the secondary cooling radiator example occurred at the lowest tube inside diameter of all three examples. The secondary cooling radiator example had also the lowest volumetric flow in each tube. The Brayton cycle radiator example, having the largest volumetric flow rate per tube, yielded the absolute minimum weight at the largest tube inside diameter.

Another noteworthy characteristic of these minimum weight radiators is the magnitude of fin-tube profile ratios. The secondary cooling radiator example has the lowest temperature level and the largest L/R_o, while the Rankine cycle radiator example has the largest temperature level and the smallest L/R_o of all three examples.

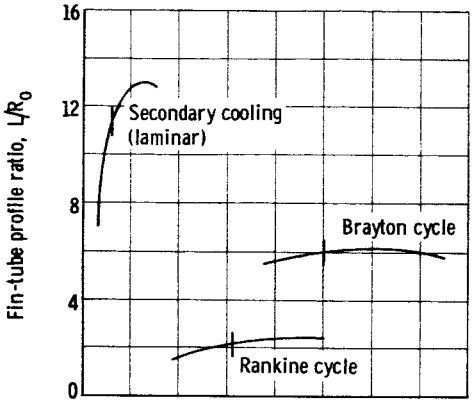

(a) Fin-tube profile ratio.

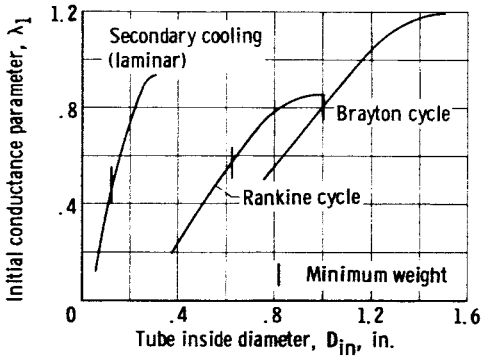

(b) Initial conductance parameter.

Figure 25. - Comparison of initial conductance parameter and fin-tube profile ratio at minimum weight for three radiator examples.

For the three radiator examples, it appeared that the initial conductance parameter at minimum weight increased with tube inside diameter. These trends and the variations of fin-tube profile ratio at minimum weight for each diameter and absolute minimum weight are further illustrated in figure 25 for the examples considered.

Design trade-offs. - It is seen from comparison of total weight and panel planform area curves (figs. 9(a) and (b), p. 19, Rankine cycle radiator example, 14(a) and (b), p. 23, secondary cooling radiator example, and 19(a) and (b), p. 27, Brayton cycle radiator example) that total weight first decreases with increasing tube inside diameter until the minimum points are reached, while panel planform area in all cases continues to increase with increasing tube inside diameter. This suggests that the use of diameters smaller than those for minimum weight affords a possible area-weight trade-off. For example, going to smaller tube inside diameters and increasing the weight by only approximately 1 percent reduces the panel planform area approximately from 4 to 8 percent, the largest reduction occurring for the Rankine cycle radiator example and the smallest for the Brayton cycle radiator example. This area-weight trade-off, however, causes an increase in aspect ratio from 50 to 65 percent.

The aspect ratio can be reduced, and at the same time similar area-weight trade-offs can be accomplished, as in the previous case, by using smaller values of L/R_o and λ_1 than those corresponding to minimum weights for the particular example instead of smaller tube inside diameters. Furthermore, the aspect ratio can also be controlled by varying the allowable pressure drop as was mentioned previously. Another means of reducing the aspect ratio is by dividing one panel into a number of smaller panels. For example, by using two panels, the aspect ratio for a Brayton cycle radiator example can be reduced from 0.76 to 0.38. In this example, the panels were imagined to be arranged around a central column, all in one plane, so that no mutual radiation or occlusion from meteoroids need be considered.

It was observed earlier (fig. 8, p. 18) that the values of L/R_o and λ_1 can have wide variations with only small affects on weight. This is further illustrated in figure 26, which shows zones of minimum weight plus 1 percent as a function of L/R_o and λ_1 for all three examples, each for the tube inside diameter that gave the smallest total weight. In addition, the panel planform area varies directly with L/R_o and λ_1 as with D_{in}. This implies that the lowest panel planform area within the zones shown in figure 26 can be expected

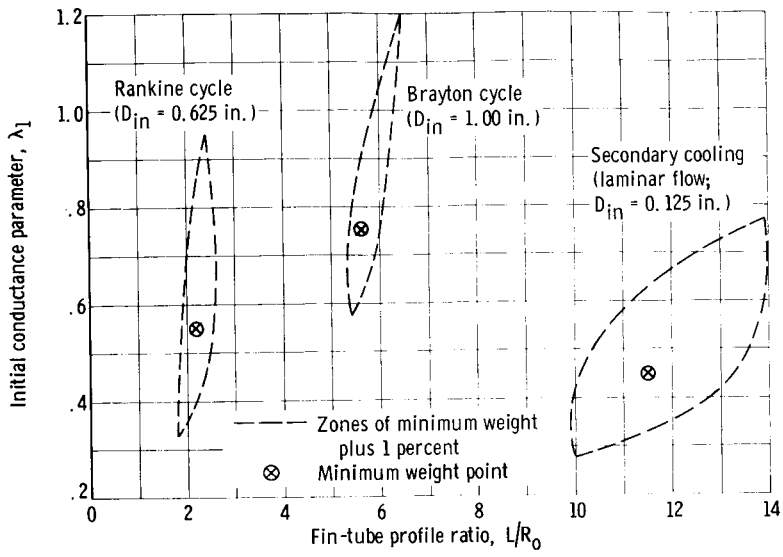

Figure 26. - Comparison of fin-tube profile ratios and initial conductance parameters of three radiator examples for zones of minimum weight plus 1 percent.

at values of L/R_o and λ_1 at the lower tip of the zones. In this case, the area reduction, compared with the values at minimum weight, was approximately 5 to 9.5 percent, and the reduction in aspect ratio was approximately 4 to 12 percent.

Flow regimes. - The factors that determine whether laminar or turbulent flow result are the magnitude of the mass flow rate (which is directly proportional to the heat-rejection rate), the fluid dynamic viscosity, and the tube diameter. In the high heat-rejection-rate Rankine cycle radiator example, the liquid metal NaK showed the highest Reynolds number, mainly a result of the highest mass flow rate of all three examples. Argon, used in the low heat-rejection-rate Brayton cycle radiator example, was turbulent as a result of the lowest dynamic viscosity despite the lowest mass flow rate. On the other hand, the ether (ET-378) in the secondary cooling radiator example has a very high viscosity (about 200 times as high as argon) but relatively small mass flow rate. This yielded a flow in the laminar region for the minimum weight radiator, which had relatively small tube diameter. At higher tube diameters in secondary cooling radiators, the radiator design may become difficult because of the uncertainty involved in the transition heat transfer and friction relations. In general, turbulent flow gives lighter radiators than laminar flow for a given tube inside diameter, if such a flow can be accomplished by some type of turbulators. The turbulators, however, will cause additional pressure losses and demand more pumping power. Consequently, in order to dissipate the additional heat load caused by additional pump power, larger flow rates in the radiator may be required. Therefore, the added penalties for the apparent saving in radiator weights resulting from the use of turbulators should be carefully studied.

CONCLUDING REMARKS

The analysis, equations, and procedures developed herein can be utilized

for determining design configurations or parametric studies of flat-plate central-fin-tube sensible-heat radiators for a wide range of power system applications. Sample calculations conducted for single representative Rankine cycle, secondary cooling, and Brayton cycle radiators showed that unique conditions can be defined for minimum weight configurations and that a wide range of radiator geometry can be obtained with relatively small variation in total weight. Each radiator example revealed somewhat different thermal and physical characteristics that were attributable to the particular range of heat-rejection rate, temperature level, temperature difference, and type of working fluid. However, a more extensive series of parametric studies covering a wide range of input parameters will be required to define the characteristics of these classes of radiators better.

Lewis Research Center,
National Aeronautics and Space Administration,
Cleveland, Ohio, February 15, 1965.

APPENDIX A

SYMBOLS

A	area, sq ft
a	finite plate thickness and spalling factor
$\overline{C}$	occlusion factor
C,C'	constants of integration
c	sonic velocity, ft/sec
c_p	constant pressure specific heat, Btu/(lb)($^{\circ}$R)
D	diameter, ft
F	angle factor
F_o	integrated friction parameter
f	friction coefficient
G	mass velocity, lb/(sec)(sq ft)
g	conversion factor, 32.2 (ft/sec^2)(lb mass/lb force)
H	header length, ft
h	heat-transfer coefficient, Btu/(sec)(sq ft)($^{\circ}$R)
j	location
K	constant
k	thermal conductivity of tube and fin material, Btu/(hr)(ft)($^{\circ}$R)
k_w	thermal conductivity of working fluid, Btu/(sec)(ft)($^{\circ}$R)
L	half-fin width
$\dot{m}$	mass flow rate, lb/sec
N	number of tubes
N_c	blackbody conductance parameter, dimensionless
n	number of elemental isothermal strips

P	pressure, lb/sq ft abs
$P(0)$	overall probability of no meteoroid penetration
Pr	Prandtl number
$\bar{p}$	total number of identical panels
$p(0)$	probability of no meteoroid penetration of a segment
$\bar{p}_s$	number of identical panels surviving
Q	heat-rejection rate, Btu/hr or Btu/sec
R	gas constant, ft-lb/(lb)($^{\circ}$R)
R_A	aspect ratio
Re	Reynolds number
R_o	tube outside radius, ft
r	index of summation
T	absolute temperature, $^{\circ}$R
t	fin thickness, ft
U_o	overall heat-transfer coefficient, Btu/(hr)(sq ft)($^{\circ}$R)
V	velocity, ft/sec
$\bar{V}$	average meteoroid velocity, 98 400 ft/sec
W	weight, lb
$\bar{X}$	distance from base surface along fin width, dimensionless
x	distance along header length, ft
Z	tube length, ft
z	distance in direction of fluid flow in tubes, ft
α	constant in meteoroid mass distribution, 0.53×10^{-10} gm$^{\beta}$/(sq ft)(day)
β	constant in meteoroid mass distribution, 1.34
δ	wall thickness, ft
ϵ	hemispherical emissivity

$\bar{\epsilon}$ apparent emissivity

η fin-tube effectiveness

θ temperature ratio, dimensionless

λ conductance parameter, dimensionless

μ viscosity, lb/(ft)(sec)

ρ density, lb/cu ft

σ Stefan-Boltzmann constant, 1.713×10^{-9} Btu/(sq ft)(hr)($^{\circ}R^4$)

τ mission time, days

Subscripts:

a armor

C convection

c liner

e exposed

F fin

f exit

H header

I liquid content

i inlet

in inside

j at location j; radiator element

L liquid

n last element

o outside or outlet

P panel

p particle

R radiated

r	radiator
S	sensible
s	sink
sc	subcooled
t	tube
tot	total
v	vulnerable
vap	vapor
w	working fluid
$\underline{\bar{X}}$	at location $\underline{\bar{X}}$
x	at location x
1	first element
2	second element

APPENDIX B

ARMOR THICKNESS AND VULNERABLE AREA

The tube armor thickness δ_a has to be sufficient to assure the desired probability of no meteoroid puncture during the prescribed mission time. The armor thickness required to give this protection was computed by the following formula taken from reference 17

$$\delta_a = 2a\left(\frac{62.45}{\rho_t}\rho_p\right)^{1/2}\left(\frac{\overline{V}}{c}\right)^{2/3}\left(\frac{6.747\times10^{-5}}{\rho_p}\right)^{1/3}\left\{\frac{\tau\alpha A_v}{[-\ln P(0)](\beta+1)}\right\}^{1/3\beta} \tag{B1}$$

where

ρ_p 0.44 g/cc

$\overline{V}$ 98 400 ft/sec

β 1.34

α 0.53×10^{-10} $g^{\beta}/(\text{sq ft})(\text{day})$ (Whipple value without Earth shielding)

The coefficient a in equation (B1) stands for finite plate thickness and spalling factor, and was assigned a value of 1.75 (ref. 17). The vulnerable area A_v in equation (B1) is a product of occlusion factor $\overline{C}$ and exposed area A_e:

$$A_v = \overline{C}A_e$$

The factor $\overline{C}$ represents reduction in armor thickness due to shielding of discrete surfaces. In this analysis, $\overline{C}$ was taken to be equal to 1; that is, no shielding was assumed.

The exposed area A_e is considered to consist of the tube outside surface area A_t and the header outside surface area A_H. The elemental tube outside area at location j is obtained from equations (1) and (3) as:

$$(\Delta A_t)_j = \frac{3600\dot{m}c_p(\Delta T)}{U_o(T_j - T_{o,j})} \tag{B2}$$

The total tube outside area is obtained by summing equation (B2) over the index j:

$$A_t = \sum_{j=1}^{n}(\Delta A_t)_j = \pi D_o N Z \tag{B3}$$

The tube outside diameter D_o is a function of tube inside diameter D_{in}, tube armor thickness δ_a, and liner thickness δ_c:

$$D_o = D_{in} + 2\delta_a + 2\delta_c \tag{B4}$$

The tube inside diameter was an input for this analysis. It is one of the quantities that is varied parametrically to study the effect on radiator design, panel planform area, and weight.

The thickness of the liner was scheduled with inside diameter by the following relation

$$\delta_c = 0.04\ D_{in} \tag{B5}$$

with a minimum thickness of 0.015 inch.

At this point in the program the header area is unknown. Since header area is taken as a part of vulnerable area, an estimated value for the total vulnerable area must be used initially in equation (B1) when the header area is nonnegligible. Equations for determining header area are given in appendix E. An iteration is incorporated into the program to determine actual total vulnerable area when the header area is significant.

APPENDIX C

PRESSURE DROP IN RADIATOR TUBES

The change in pressure due to the flow of fluid in the radiator tubes can be divided into three components: the loss in pressure when the fluid is turned from the header into the tube and from the tube into the header; the momentum pressure rise associated with the density and velocity changes as the fluid flows down the tube; and the pressure loss due to friction. In this analysis the first two components have been ignored, and the calculated pressure drop was based on the pipe friction only. The turning loss was ignored because the velocities of single phase fluids in the tubes are relatively small, and it has been further assumed that the header-tube joints are smooth and rounded. Under such conditions, the turning losses amount to less than one dynamic head at the tube entrance, whereas the friction pressure loss may be several dynamic heads. With relatively small changes in velocity in the tubes for the gas working fluid, and no change for the liquid working fluid, the momentum change is considerably less than one dynamic head and can also be ignored. Furthermore, the two pressure changes are of opposite sign and tend to cancel each other. Should circumstances arise so that it is desirable to consider turning losses, this can be done merely by reducing the allowable pressure drop in the tubes.

To obtain the friction pressure drop in a radiator tube it is necessary to integrate the Fanning equation

$$dP = -2f\rho \frac{V^2}{g} \frac{dz}{D_{in}} \tag{C1}$$

over the entire tube length. In this analysis, f has been assumed constant along the tube and is based on the Reynolds number in the tube. The friction coefficient f in equation (C1) is evaluated for turbulent flow ($Re \geq 3000$) as

$$f = \frac{0.046}{Re^{0.2}} \tag{C2a}$$

and for laminar flow ($Re \leq 2300$) as

$$f = \frac{16}{Re} \tag{C2b}$$

Two friction factors and two pressure drops are computed for $2300 < Re < 3000$, from the laminar and turbulent flow equations, when comparative results in this transitional region are required. The integration of the Fanning equation is dependent on the nature of the working fluid.

Liquid Working Fluid

If the working fluid is a liquid, the integration of equation (C1)

presents no problem because the variation of both the liquid density and flow velocity with temperature is comparatively small. The liquid density can be considered constant over the entire tube length (constant diameter tubes) and evaluated at the temperature of tube midpoint. The integrated form of the equation becomes

$$P_f - P_i = -2f\rho_L \frac{V^2}{g} \frac{Z}{D_{in}} \tag{C3}$$

Gas Working Fluid

When the fluid in the radiator tube is a gas, the problem of computing the pressure drop becomes more difficult because the assumption of constant density and velocity, in general, can no longer be applied. The extraction of heat from the gas through the convection-conduction-radiation process increases the density of the gas along the tube length to a much greater extent than for liquids. Equation (C1) can be rewritten in terms of gas temperatures

$$dP = -2f \frac{G^2}{gD_{in}} \frac{RT_j}{P} dz \tag{C4}$$

where $G = 4\dot{m}/\pi D_{in}^2 N$. Equation (C4) can be integrated as soon as an analytical relation between temperature and tube position can be determined.

Such a relation in differential form is available by equating the right sides of equations (1) and (3), or equations (1) and (8):

$$\frac{dT_j}{dz} = \left(\frac{\pi D_o N U_o}{3600\dot{m}c_p}\right)\left(T_j - T_{o,j}\right) = \left[\frac{4\sigma\epsilon R_o N\left(1 + \frac{L}{R_o}\right)\eta_j}{3600\dot{m}c_p}\right]\left(T_{o,j}^4 - T_s^4\right) \tag{C5}$$

This relation is not very convenient because, at the point in the computer program where it is required, D_o, N, and U_o are all unknowns.

In order to avoid the use of another equation, namely equation (C5), which involved quantities that had to be determined by an iterative process, it was assumed for convenience that the rate of change of fluid temperature with tube length followed the relation

$$dT_j = K\left(T_j^4 - T_s^4\right)dz \tag{C6a}$$

so that

$$\int dz = \frac{1}{K} \int \frac{dT_j}{T_j^4 - T_s^4} + C \tag{C6b}$$

where C is the constant of integration. The relation between fluid temperature T_j and tube position z is now obtained by integrating the indefinite integrals in equation (C6b) to give

$$z = -\frac{1}{2KT_s^3}\left(\coth^{-1}\frac{T_j}{T_s} + \tan^{-1}\frac{T_j}{T_s}\right) + C \tag{C7}$$

where the constant of integration C is evaluated at the initial conditions; that is, $T_j = T_i$ when $z = 0$. The constant K can be evaluated by integrating equation (C6a) between the fluid inlet and exit temperatures, T_i and T_f, respectively:

$$K = \frac{1}{2ZT_s^3}\left\{\tanh^{-1}\left[\frac{T_s(T_f - T_i)}{T_iT_f - T_s^2}\right] + \tan^{-1}\left[\frac{T_s(T_i - T_f)}{T_iT_f + T_s^2}\right]\right\} \tag{C8}$$

When the sink temperature T_s in equation (C7) takes the value of zero, it can be shown, for example, by expanding the hyperbolic arc cotangent and arc tangent terms into series, that equation (C7) reduces to

$$z = -\frac{1}{3KT_j^3} + C' \tag{C9}$$

Similarly, the constant K as given by equation (C8) reduces to

$$K = \frac{1}{3Z}\left(\frac{1}{T_i^3} - \frac{1}{T_f^3}\right) \tag{C10}$$

The graphical presentation of equations (C7) and (C9) is compared in figures 27(a) and (b) with actual variations of fluid temperatures based on heat-transfer considerations for a gas cycle radiator example of 0° and 400° R sink temperatures. The actual temperatures were obtained from an integration of equation (C5). Comparison of the curves indicates that the assumptions expressed in the relation (C6) result in lower local fluid temperatures than the actual values in both sink temperature cases. However, the 0° sink temperature equations (C9) and (C10) gave better temperature approximations than equations (C7) and (C8), which include the sink temperature.

The local temperatures as obtained from equations (C9) and (C10) were less than those obtained from the heat-transfer calculations by 0 to 5 percent. Reference to equation (C4) indicates that such an error in fluid temperature will result in a calculated pressure gradient that will be low by the same percentage. The error in integrated pressure drop, however, will be less than the maximum error in local fluid temperatures. Therefore, no further attempt was made to improve the accuracy of the temperature profile over that given by equations (C9) and (C10).

Equation (C4), which expresses the rate of change of the pressure, can now

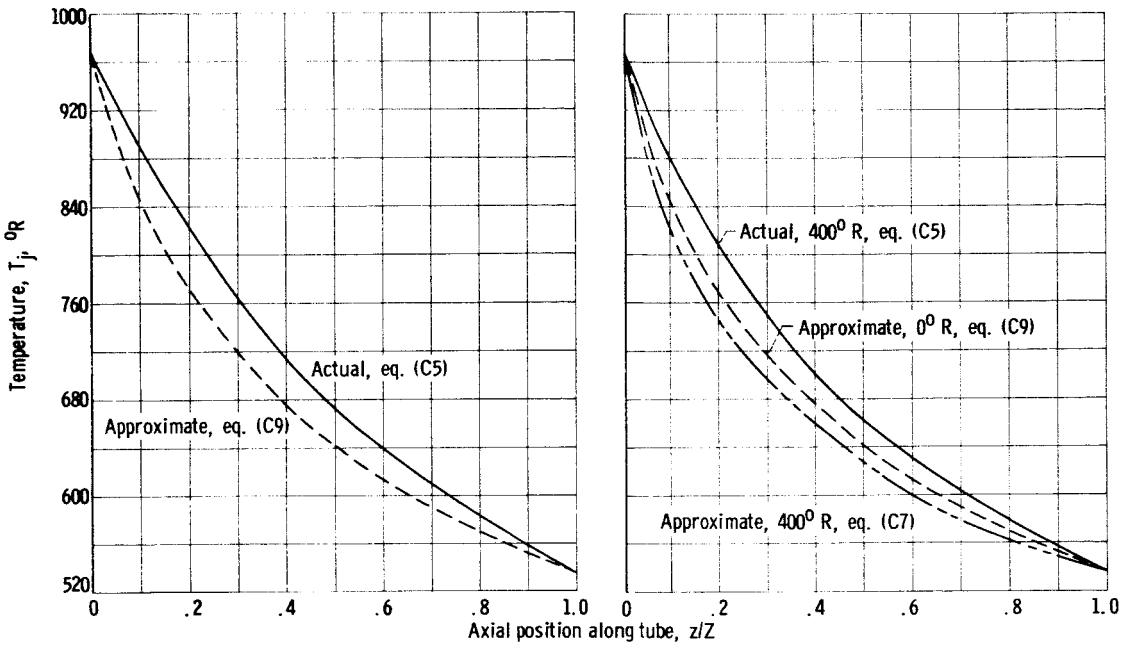

(a) Actual and approximate variations for sink temperature of 0^0 R.

(b) Actual and approximate variations for sink temperature of 400^0 R.

Figure 27. - Comparison of axial variations in gas temperature.

be transformed into a function of fluid temperature T_j alone, with the aid of equation (C6) with T_s set equal to zero:

$$P\,dP = -2f\,\frac{G^2R}{gD_{in}K}\,\frac{T_j\,dT_j}{T_j^4} \tag{C11}$$

where the constant K is obtained from equation (C10). Integration of equation (C11) between inlet and exit pressures, P_i and P_f, respectively, and between inlet and exit temperatures, T_i and T_f, respectively, yields

$$\frac{1}{2}(P_i + P_f)(P_i - P_f) = \frac{fG^2R}{gD_{in}K}\left(\frac{1}{T_i^2} - \frac{1}{T_f^2}\right) \tag{C12a}$$

Inasmuch as the difference between the inlet and exit pressures is generally small for Brayton cycle gas radiators, it can be assumed that

$$\frac{1}{2}(P_i + P_f) \equiv P_i$$

Equation (C12a) can then be reduced to the form

$$\frac{\Delta P}{P_i} = \frac{fG^2R}{P_i^2 gD_{in}K}\left(\frac{1}{T_i^2} - \frac{1}{T_f^2}\right) \tag{C12b}$$

APPENDIX D

GEOMETRY OF TUBES AND FINS

The heat-transfer analysis and the armor-thickness calculations in appendix B have established all necessary relations to describe the geometric details of the radiator panel tubes and fins, with the exception of the tube length Z. Thus, equations (B1), (B4), and (B5) gave the tube armor thickness δ_a, tube outside diameter D_o, and the liner thickness δ_c, respectively. The half-fin width is available from the equation

$$L = \frac{L}{R_o} 0.5\ D_o \tag{D1}$$

and the fin thickness follows from equation (12) as

$$t = \frac{2\sigma\epsilon T_{o,j}^3 L^2}{k_F \lambda_j} \tag{D2}$$

Tube Length in Turbulent Flow

For inert gases in turbulent flow, the length of a single tube Z is obtained from equation (C12b):

$$\frac{\Delta P}{P_i} = \frac{fG^2 R}{P_i^2 g D_{in} K}\left(\frac{1}{T_i^2} - \frac{1}{T_f^2}\right)$$

With the use of the definitions

$$G = \frac{4\dot{m}}{\pi D_{in}^2 N} \tag{D3}$$

and

$$Re = \frac{4\dot{m}}{\pi D_{in} N \mu}$$

the constant K obtained from equation (C10), and the friction coefficient f from equation (C2a), equation (C12b) then takes the form

$$\left(\frac{\Delta P}{P_i}\right)_t = \left(\frac{\dot{m}}{20.3\ N}\right)^{1.8} \frac{R T_i F_o Z}{P_i^2}\ \mu^{0.2}\left(\frac{1}{D_{in}}\right)^{4.8} \tag{D4}$$

where

$$F_o = 1.5\left(\frac{T_f}{T_i}\right)^3\left[\frac{1 - \left(\frac{T_i}{T_f}\right)^2}{1 - \left(\frac{T_i}{T_f}\right)^3}\right] \tag{D5}$$

Substituting $N = NZ/Z$ for the number of tubes in equation (D4) and solving for the tube length Z give the following relation:

$$Z = \left(\frac{20.3\ NZ}{\dot{m}}\right)^{9/14}\left[\frac{P_i^2\left(\frac{\Delta P}{P_i}\right)_t}{RT_iF_o}\right]^{5/14}\left(\frac{1}{\mu}\right)^{1/14}\left(D_{in}\right)^{12/7} \tag{D6}$$

By similar manipulations of equation (C3), the tube length Z of sensible-heat radiator tubes that contains liquids or liquid metal fluids is

$$Z = \left(\frac{20.3\ NZ}{\dot{m}}\right)^{9/14}\left[\rho_L(\Delta P)_t\right]^{5/14}\left(\frac{1}{\mu}\right)^{1/14}\left(D_{in}\right)^{12/7} \tag{D7}$$

Tube Length in Laminar Flow

When the gas flow in the tubes is laminar, equation (C12b) can be rearranged similarly to equation (D4) except for the friction coefficient f, which is obtained from equation (C2b)

$$\left(\frac{\Delta P}{P_i}\right)_t = \frac{\dot{m}}{0.7903\ N}\frac{RT_iF_oZ}{P_i^2}\mu\left(\frac{1}{D_{in}}\right)^4 \tag{D8}$$

where F_o is given by equation (D5). The relation for the tube length Z, in terms of the product NZ, is

$$Z = \left[\frac{0.7903\ NZ}{\dot{m}}\frac{P_i^2\left(\frac{\Delta P}{P_i}\right)_t}{RT_iF_o}\frac{1}{\mu}D_{in}^4\right]^{0.5} \tag{D9}$$

Similarly, for liquids and liquid metals in laminar flow, equation (C3) becomes

$$(\Delta P)_t = \frac{\dot{m}}{0.7903\ N}\frac{Z}{\rho_L}\mu\left(\frac{1}{D_{in}}\right)^4 \tag{D10}$$

and tube length Z is obtained in terms of NZ from

$$Z = \left[\frac{0.7903\ NZ}{\dot{m}}\ \rho_L(\Delta P)_t\ \frac{1}{\mu}\ D_{in}^4\right]^{0.5} \tag{D11}$$

Number of Tubes

With tube length Z determined by equations (D6), (D7), (D9), or (D11), depending on the phase of the working fluid (gaseous or liquid) and flow regime (turbulent or laminar), the number of tubes N can be calculated from the product NZ (eq. (B3)). In this program, fractional numbers of tubes were rounded off to the next higher integers.

Panel Area and Aspect Ratio

The panel planform area, which is the projected area of the fins and tubes, is given by

$$A_P = HZ = D_O NZ\left(1 + \frac{L}{R_O}\right) \tag{D12}$$

The aspect ratio, defined as the ratio of the panel width to the tube length, can be obtained from the preceding equation for panel area and the appropriate equation for tube length Z, that is, equation (D6), (D7), (D9), or (D11) to give

$$R_A = \frac{H}{Z} = \frac{A_P}{Z^2} \tag{D13}$$

APPENDIX E

HEADER DESIGN

A comprehensive study of flat sensible-heat space radiators requires the inclusion of a design for the inlet and outlet headers. A detailed development of the equations that affect header geometry, shape, vulnerable area, and weight is given in this section. In the analysis, it is assumed that the headers are joined directly to the tubes in the same plane as the tubes. Accordingly, they are exposed to meteoroid impact and are protected with the same armor thickness as the tubes. Because the shape and size of the headers depend on the phase of the fluid, it was necessary to consider the header design for the two types of fluid separately. Mass flow rate, pressure level, pressure drop, temperature level, and header length were treated as independent variables for the header design in all cases. Radiation from the outer surfaces of the headers was assumed negligible. The justification for this assumption is discussed later.

Gas Headers

The header shape and arrangement employed for a single-panel radiator that uses inert gas as a working fluid is shown in figure 1(a). The gas is taken into the inlet header at one side of the radiator, is distributed among the panel tubes, and leaves the outlet header at the opposite side of the radiator panel. This type of design tends to approach an equal pressure drop across each tube, thereby promoting uniform flow distribution and similar velocity profiles in both headers.

Diameter and pressure drop. - The variation in header diameter with longitudinal position along the header was assumed to be given by the following relation:

$$D_x = D_{i,H}\left(1 - \frac{x}{H}\right)^{1/3} \tag{E1}$$

This approach follows the procedure for a minimum weight header suggested by AiResearch Manufacturing Division of The Garrett Corporation, Phoenix, Arizona.

Because the headers are required to deliver the radiator fluid mass flow with a prescribed pressure drop, an analysis involving the friction pressure drop is used to size the inlet and outlet header diameters. Over an elemental length dx of the inlet header (fig. 1(a)), the pressure drop for the fluid in the header is given by

$$dp = -\frac{2fG_x^2\,dx}{gD_x\rho} \tag{E2}$$

The expression for the friction factor f, assumed for simplicity to be constant, will be developed in a succeeding section of this appendix. The local mass velocity is given by

$$G_x = \frac{4\dot{m}_x}{\pi D_x^2} \tag{E3}$$

It is assumed that the mass flow rate is distributed equally among the tubes in the radiator panel, or

$$\dot{m}_x = \dot{m}\left(1 - \frac{x}{H}\right) \tag{E4}$$

By inserting equations (E1), (E3), and (E4) into equation (E2) and integrating between the limits of zero and H (fig. 1(a)), where

$$H = ND_o\left(1 + \frac{L}{R_o}\right) \tag{E5}$$

the following relation between inlet-header pressure drop and inlet-header maximum diameter can be developed:

$$(\Delta P)_H = \frac{0.0755\ f\dot{m}^2 HRT_i}{P_i D_{i,H}^5} \tag{E6}$$

If equation (E6) is solved for the inlet-header maximum diameter

$$D_{i,H} = \left[\frac{0.0755\ f\dot{m}^2 HRT_i}{\left(\frac{\Delta P}{P_i}\right)_H P_i^2}\right]^{0.2} \tag{E7}$$

Likewise, for the outlet header,

$$D_{o,H} = \left[\frac{0.0755\ f\dot{m}^2 HRT_f}{\left(\frac{\Delta P}{P_i}\right)_H P_i P_f}\right]^{0.2} \tag{E8}$$

If it is assumed that the pressure-drop fractions in the two headers are the same, then, from equations (E7) and (E8), it follows that

$$D_{o,H} = D_{i,H}\left(\frac{P_i T_f}{P_f T_i}\right)^{0.2} \tag{E9}$$

For this particular analysis, it was also assumed that the only pressure

drop between the two headers was the frictional pressure loss in the tubes. Accordingly,

$$P_f = P_i\left[1 - \left(\frac{\Delta P}{P_i}\right)_t - \left(\frac{\Delta P}{P_i}\right)_H\right] \tag{E10}$$

Friction factor. - The representative value of the friction factor f in equations (E7) and (E8) was obtained as the value of f at the middle section of the header (x/H = 0.5). From the assumption expressed by equation (E4), it follows that, at the midpoint,

$$\dot{m}_x = 0.5\ \dot{m} \tag{E11}$$

It is also assumed, and this assumption has been borne out by the results of this analysis, that the flow is always turbulent at the middle section of the header. Therefore, the empirical relation

$$f = \frac{0.046}{Re_x^{0.2}} \tag{E12}$$

can be used provided that

$$Re_x = \frac{4\dot{m}_x}{\pi D_x \mu} \tag{E13}$$

is the local Reynolds number. Combining equations (E1), (E11), (E12), and (E13) yields

$$f = 0.048\left(\frac{D_{i,H}\mu}{\dot{m}}\right)^{0.2} \tag{E14}$$

Substituting the expression for $D_{i,H}$ from equation (E7) into equation (E14) yields, for the inlet header:

$$f_{i,H} = 0.0382\left(\frac{\mu}{\dot{m}^{0.6}}\right)^{0.208}\left[\frac{HRT_i}{\left(\frac{\Delta P}{P_i}\right)_H P_i^2}\right]^{0.0416} \tag{E15}$$

The corresponding expression for the outlet header, from the use of equation (E8), becomes

$$f_{o,H} = 0.0382\left(\frac{\mu}{\dot{m}^{0.6}}\right)^{0.208}\left[\frac{HRT_f}{\left(\frac{\Delta P}{P_i}\right)_H P_i P_f}\right]^{0.0416} \tag{E16}$$

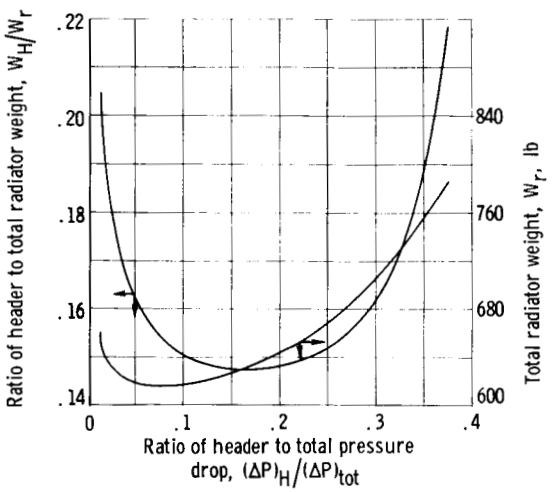

Figure 28. - Effect of header pressure drop on radiator weight for Brayton cycle radiator example. Tube inside diameter, 1.0 inch; initial conductance parameter, 1.0; fin-tube profile ratio, 6.0; total pressure drop, 0.08.

The difference between inlet and exit pressures P_i and P_f, respectively, is generally small. On the other hand, the inlet temperature T_i may be as much as twice the exit temperature T_f. For this condition the friction factor ratio $f_{i,H}/f_{o,H}$ is about 1.03. Therefore, for simplicity, equation (E15) was used for the friction factor in both the inlet and outlet headers.

Pressure-drop fraction. - In most radiator applications the pressure drop across the entire radiator is usually set by considerations other than radiator design, but the distribution of this pressure drop between the headers and the tubes may be left to the discretion of the radiator designer. A criterion for the selection of the pressure drop in the header is illustrated by a Brayton cycle radiator example with the tube inside diameter, initial conductance parameter, and fin-tube profile ratio fixed at 1 inch, 1.0, and 6.0, respectively. Calculations were conducted in which the pressure-drop fraction in the header $(\Delta P/P_i)_H$ was varied, while the fraction across the entire radiator $(\Delta P/P_i)_{tot}$ was maintained constant at 0.08. The results of the calculations are shown in figure 28. It is seen from the figure that the radiator weight is minimized when the pressure drop in each header is a little less than 10 percent of the total radiator pressure drop. Therefore in the Brayton cycle radiator calculations, the pressure drop in each header was taken to be 10 percent of the total allowable pressure drop (see table I, p. 15).

Weight. - The weight of the header wall element dx in figure 1(a), (p. 4) is given by

$$dW_{i,H} = \left[\rho_H(D_x + 2\delta_c + \delta_a)\delta_a + \rho_c(D_x + \delta_c)\delta_c\right]\pi\, dx \qquad \text{(E17)}$$

Substituting equation (E1) into equation (E17) and expressing the header length coordinate in nondimensional form x/H yield

$$dW_{i,H} = \pi H\left\{\rho_H\left[D_{i,H}\left(1 - \frac{x}{H}\right)^{1/3} + 2\delta_c + \delta_a\right]\delta_a + \rho_c\left[D_{i,H}\left(1 - \frac{x}{H}\right)^{1/3} + \delta_c\right]\delta_c\right\}d\left(\frac{x}{H}\right) \qquad \text{(E18)}$$

Integration of equation (E18) between $0 \le x/H \le 1$ yields the weight of the inlet header:

$$W_{i,H} = \pi H\left[(0.75\, D_{i,H} + 2\delta_c + \delta_a)\delta_a\rho_H + (0.75\, D_{i,H} + \delta_c)\rho_c\delta_c\right] \qquad \text{(E19)}$$

The weight of the outlet header is obtained in a similar manner, and is given as

$$W_{o,H} = \pi H\left[(0.75\ D_{o,H} + 2\delta_c + \delta_a)\delta_a\rho_H + (0.75\ D_{o,H} + \delta_c)\rho_c\delta_c\right] \tag{E20}$$

The combined weight of the inlet and outlet headers is

$$W_H = \pi H\left\{\left[0.75(D_{i,H} + D_{o,H}) + 4\delta_c + 2\delta_a\right]\delta_a\rho_H + \left[0.75(D_{i,H} + D_{o,H}) + 2\delta_c\right]\rho_c\delta_c\right\} \tag{E21}$$

Vulnerable area. - The vulnerable area of the headers for the configurations shown in figures 1 and 2 was taken as the outside surface area of the headers. The outside area of the inlet header is calculated by integrating the differential area over the header length (fig. 1(a))

$$\left(A_{o,H}\right)_i = \pi H \int_0^1 \left[D_{i,H}\left(1 - \frac{x}{H}\right)^{1/3} + 2\delta_a + 2\delta_c\right] d\left(\frac{x}{H}\right) \tag{E22}$$

or

$$\left(A_{o,H}\right)_i = \pi H(0.75\ D_{i,H} + 2\delta_a + 2\delta_c) \tag{E23}$$

A similar expression is obtained for the outside area of the outlet header:

$$\left(A_{o,H}\right)_o = \pi H(0.75\ D_{o,H} + 2\delta_a + 2\delta_c) \tag{E24}$$

The total outside area for both headers is then

$$\left(A_H\right)_o = \pi H\left[0.75(D_{i,H} + D_{o,H}) + 4(\delta_a + \delta_c)\right] \tag{E25}$$

However, the armor thickness δ_a is unknown (see appendix B). Therefore, to eliminate the need of another set of iterations, the vulnerable area of the headers was assumed, for simplicity, in this analysis to be given by

$$A_H = 0.75\ \pi H(D_{i,H} + D_{o,H}) \tag{E26}$$

The vulnerable area of the headers from equation (E26) can then be combined with the vulnerable area of the tubes for use in equation (B1).

Radiation. - The amount of radiation from an exposed header is a function primarily of its temperature and outer surface area. In this analysis it was assumed that the surface temperatures for the inlet and outlet headers were equal to the surface temperatures of the first and last strips, respectively, into which the tubes were divided (see ANALYSIS section).

The approximate rate of heat rejection by thermal radiation from the inlet

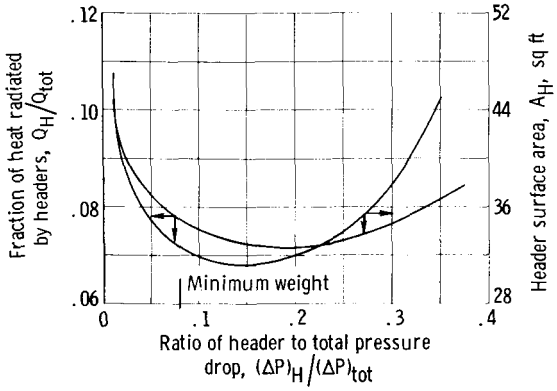

Figure 29. - Effect of header pressure drop on header surface area and header heat rejection for Brayton cycle radiator example.

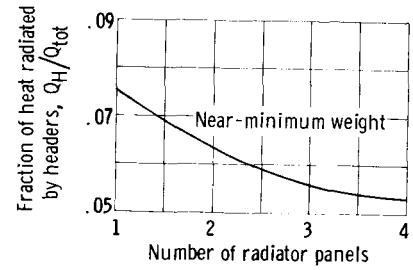

Figure 30. - Effect of paneling on heat rejection from headers for Brayton cycle radiator example.

and outlet gas headers was calculated by using the following equation:

$$Q_H = \sigma \epsilon F_H \left[\left(A_{o,H}\right)_i \left(T_{o,1}^4 - T_s^4\right) + \left(A_{o,H}\right)_o \left(T_{o,n}^4 - T_s^4\right) \right] \qquad \text{(E27)}$$

where $T_{o,1}$ and $T_{o,n}$ are the surface temperatures of the first and the last strips of the radiator panel, respectively (see fig. 2(a)). It was also assumed that the radiation from the headers does not affect the temperatures, pressures, and other properties of the gas at the radiator inlet and outlet. The surface emissivity ϵ and the equivalent sink temperature T_s were considered to be the same as for the radiation from the fins and tubes (see table I). The factor F_H equal to 0.9 was included to account for the radiant interchange between the headers, fins, and tubes. The inlet- and outlet-header surface areas $\left(A_{o,H}\right)_i$ and $\left(A_{o,H}\right)_o$, respectively, were obtained from equations (E23) and (E24), respectively.

Figure 29 illustrates the variation in the heat rejected by the headers, expressed as a fraction of the panel heat-rejection rate, and header outer surface area as a function of the header pressure-drop fraction. It is seen from the figure that for a header pressure-drop fraction near that corresponding to minimum radiator weight, the heat rejection from the headers amounts to between 7 and 8 percent of the panel heat rejection.

Calculations were also made to see what effect a division of heat load among several nonredundant and interconnected panels would have on the ratio of heat radiated by the headers. In these calculations, the radiant interchange between a header on one panel and any other header as well as mutual shielding by the headers and panels were neglected. The results of these calculations are shown in figure 30, where the fraction of heat radiated by the headers is plotted against the number of radiator panels for near-minimum-weight conditions. It is seen from the figure that the heat rejected by the headers is reduced from 7.5 to approximately 5.3 percent if four panels are used instead of one.

The preceding discussion has illustrated the magnitude of the percentage of heat radiated from the headers for a Brayton cycle radiator example, as well

as the various factors that contribute to this heat rejection. As mentioned earlier, the heat rejected from the headers was neglected in this program for simplicity. If for certain applications the thermal radiation from the headers is substantial, an approximate procedure, presented in a later part of this appendix, can be used to obtain an estimate of the effect of header radiation on the radiator geometry and weight.

Liquid Headers

The design of the headers for the radiators that use liquid or liquid metal as a working fluid was simplified by assuming that the headers were tubular with uniform diameters. Consideration was given to the use of tapered liquid headers in order to reduce the header and radiator weight. It can be shown, however, that if tapered instead of straight headers are used in both of the foregoing examples, the minimum weight of the radiator, including the weight of the liquid content in the headers, is reduced by less than 2.5 percent.

It was also assumed that the working fluid enters the inlet header at the middle and leaves the outlet header at the same position (fig. 1(b)). Such a design provides some saving in header weight, since, in such an arrangement, each half of the header handles only one-half of the total mass flow. Other arrangements, such as the U-type or Z-type headers are discussed at the end of this section.

Pressure drop. - For equal flow distribution among the tubes, the following equation should be satisfied:

$$\dot{m}_x = \frac{\dot{m}}{2} - \frac{\dot{m}x}{H_L} \tag{E28}$$

The allowable pressure-drop relation is obtained by integrating equation (E2), where the mass velocity is now evaluated from equation (E28) and the continuity equation for constant diameter as

$$G_x = \rho_L V_x = \frac{4\dot{m}\left(0.5 - \frac{x}{H_L}\right)}{\pi D_{L,H}^2} \tag{E29}$$

The friction factor with turbulent flow assumed in the headers is given by equation (C2a).

Substituting equations (E29) and (C2a) into equation (E2) makes the latter a function of one independent variable only:

$$-dp = 4.411\times10^{-3}\left(\frac{\dot{m}^{1.8}\mu^{0.2}}{D_{L,H}^{4.8}\rho_L}\right)\left(0.5 - \frac{x}{H_L}\right)^{1.8} dx \tag{E30}$$

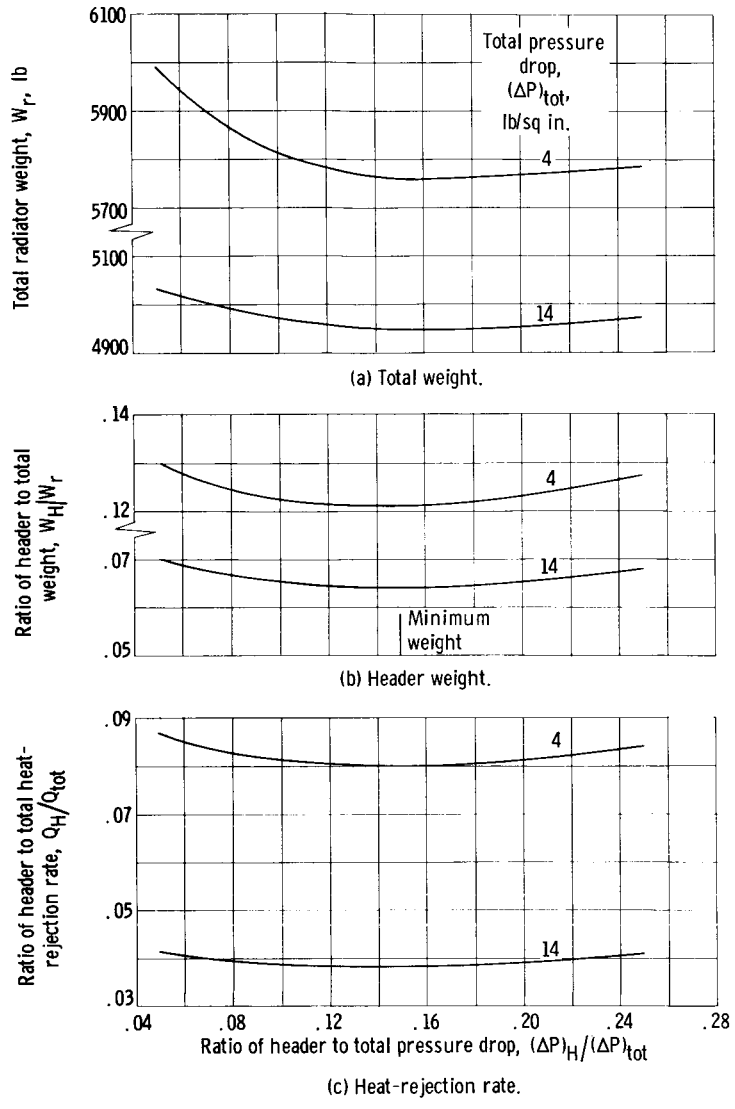

Figure 31. - Variations in radiator total and header weight and header heat-rejection rate with header pressure drop and total allowable pressure drop for Rankine cycle radiator example. Tube inside diameter, 0.625 inch; initial conductance parameter, 0.5; fin-tube profile ratio, 2.0. (See table I for other inputs.)

The integration of equation (E30) yields the desired relations between length, diameter, and pressure drop:

$$(\Delta P)_H = \frac{0.2263 \times 10^{-3} \dot{m}^{1.8} \mu^{0.2} H_L}{D_{L,H}^{4.8} \rho_L} \tag{E31}$$

When the header diameter is taken as the dependent variable, equation (E31) becomes

$$D_{L,H} = 0.174\,\dot{m}^{0.375}\mu^{0.0417}\left[\frac{H_L}{(\Delta P)_H \rho_L}\right]^{0.208} \qquad \text{(E32)}$$

Weight. - The combined weight of the inlet and outlet liquid or liquid metal headers, including armor and liner, but without liquid content, can be obtained from

$$W_{L,H} = 2\pi H\left[\rho_H \delta_a\left(D_{L,H} + 2\delta_c + \delta_a\right) + \rho_c \delta_c\left(D_{L,H} + \delta_c\right)\right] \qquad \text{(E33)}$$

where H is determined from equation (E5), δ_a from equation (B1), δ_c from equation (B5), and the inside diameter of the headers, $D_{L,H}$ is obtained from equation (E32). The material densities ρ_c and ρ_H are inputs (see table I).

Pressure-drop fraction. - An analysis similar to that for the Brayton cycle radiator example was made of the headers of the Rankine cycle radiator and the secondary cooling radiator example by calculating the effects of a change in the pressure-drop fraction in the headers on the total radiator weight and header radiation. Calculations were made for total allowable pressure drops across the entire radiator of 4 and 14 pounds per square inch. The other inputs are shown in table I. The tube inside diameters, initial conductance parameters, and fin-tube profile ratios for the calculations were taken for the near-minimum-weight condition. These values are indicated in the corresponding figures.

Figure 31(a), for the Rankine cycle radiator example, shows the variation of total radiator weight with the pressure drop in each header, the latter expressed as a ratio of total allowable pressure drop across the entire radiator. For both cases investigated (total pressure drop, 4 and 14 psi), the minimum weight occurs when the header pressure drop is approximately 15 percent of the total allowable pressure drop. This minimum value is somewhat greater than the percentage observed previously in the Brayton cycle radiator example, although there is little weight variation indicated for pressure-drop fractions between 0.10 and 0.25. It is also seen that considerable weight saving can be achieved if the allowable total pressure drop can be increased from 4 to 14 pounds per square inch (~14 percent at minimum-radiator-weight conditions). The main contributors to this weight saving are the reduced weights of the inlet and outlet headers as illustrated by the curves in figure 31(b).

Reduction in the header weights as a result of the smaller header diameters also means smaller header surfaces and therefore smaller header heat-rejection rates. The latter trends are shown by the curves in figure 31(c), which also indicate that a substantial decrease in the header heat rejection results from increasing the total allowable pressure drop. On the other hand, the increase in total pressure drop causes an increase of the fluid velocity at the tube inlet; however, the level of the fluid velocity still remains relatively small (~16 ft/sec).

The same trends as in the Rankine cycle radiator example were also observed for the secondary cooling radiator example (fig. 32). In this example, the total minimum weight occurred at a slightly lower header pressure drop

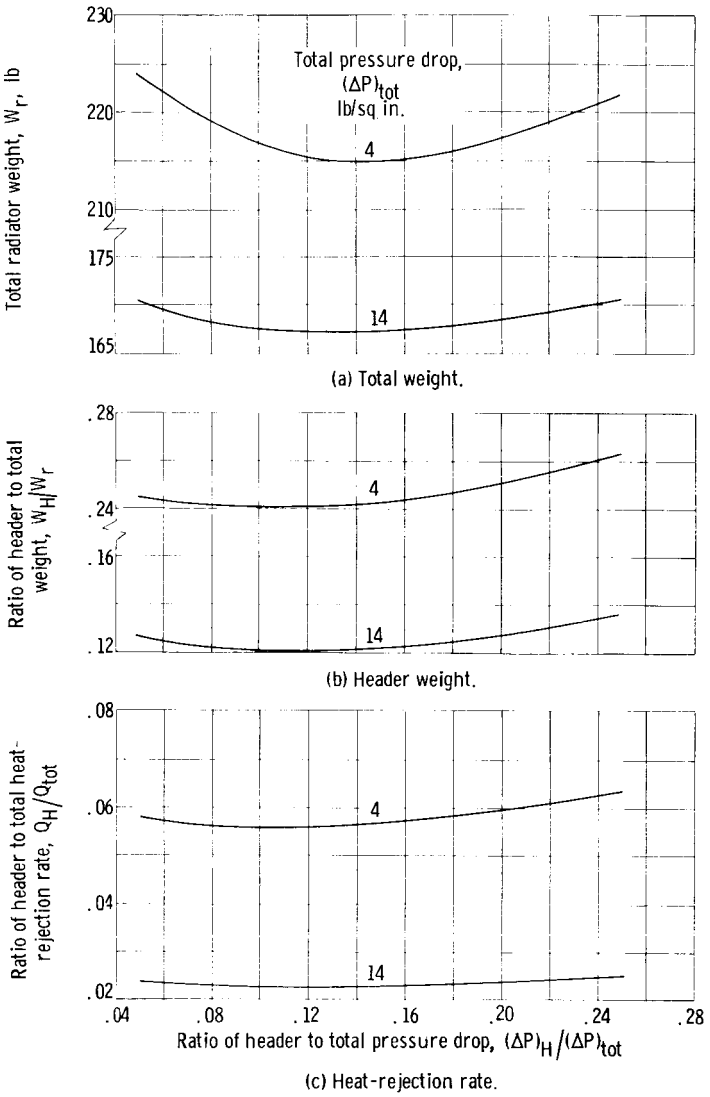

Figure 32. - Variations in radiator total and header weight and header heat-rejection rate with header pressure drop and total allowable pressure drop for secondary cooling radiator example. Tube inside diameter, 0.125 inch; initial conductance parameter, 0.5; fin-tube profile ratio, 12.0. (See table I for other inputs.)

fraction than in the Rankine case (fig. 32(a)). The total weight saving at the minimum weight is greater than in the previous example for the same increase in the total pressure drop. A similar reduction of header weight and radiation is also indicated (figs. 32(b) and (c)).

Thus far, the results of the examples considered have shown that the header radiation and weight are considerably reduced if the total pressure drop is increased and if the header pressure-drop fraction is used that minimizes the total radiator weight. The latter suggests that pressure drop considerations may have as much significance as the tube inside diameter D_{in}, initial conductance parameter λ_1, and fin-tube profile ratio L/R_o in minimizing radiator weights.

Other liquid header arrangements. - The liquid header analysis has been performed for one particular model, that is, the T-type in which the liquid enters the inlet header at the middle portion and leaves the outlet header at the same position (fig. 1(b), p. 4). This was done in order to provide some saving of the header weight. If it is required that the liquid enter and leave the radiator at one end of the headers in either a U-type or Z-type arrangement, the analysis presented in this appendix can still be used to estimate the header dimensions and weight. In U-type headers, the fluid enters and leaves the radiator at the same side, but in Z-type headers, the fluid leaves the outlet header at the opposite side of the radiator, as shown in figures 33(a) and (b). It can be shown from equation (E32) that such arrangements will increase the header diameter to approximately 1.5 times the diameter of the T-type headers (fig. 1(b)). It follows from equation (E33) that, within the accuracy of this report, the header weight will increase by approximately the same factor. The liquid content weight in the headers will increase approximately 2.25 times. It should be mentioned, however, that the increased header and liquid content weights may shift the total radiator minimum weight point (e.g., fig. 9(a), p. 19) to larger tube inside diameters. Similarly, the other two geometric parameters (λ_1 and L/R_o)

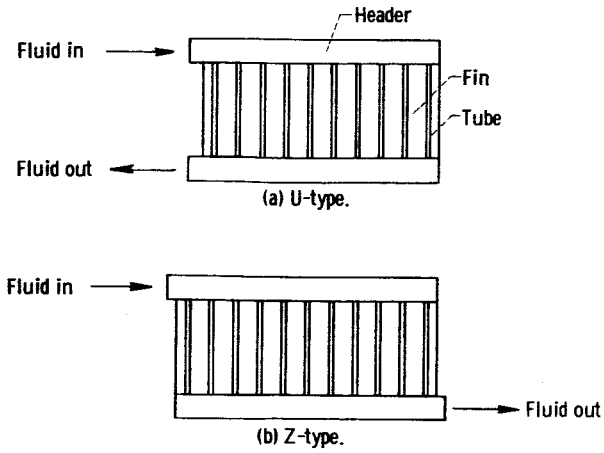

Figure 33. - Headers.

may change their values at minimum weight with a change in header arrangement.

Approximate Procedure for Non-negligible Header Radiation

The computer program described in this report neglected the header radiation for simplicity. The magnitude of this radiation has been indicated previously for several different examples. For those situations in which the thermal radiation from the headers is substantial, the following procedure may be used to obtain an estimate of the effect of header radiation on the radiator geometry and weight.

When the desired radiator dimensions are selected from the results of the program described herein, the approximate heat-rejection rate from the headers can be calculated from equation (E27) as

$$Q_H = Q_{i,H} + Q_{o,H} = \sigma \epsilon F_H \left[(A_{o,H})_i \left(T_{o,1}^4 - T_s^4 \right) + (A_{o,H})_o \left(T_{o,n}^4 - T_s^4 \right) \right]$$

where F_H, $(A_{o,H})_i$, and $(A_{o,H})_o$ are obtained as before. The header radiation thus evaluated can then be subtracted from the total radiator heat load, and the heat-rejection rate for the panel obtained is

$$Q_P = Q_{tot} - Q_H = \dot{m} c_p (T_{i,P} - T_{f,P}) \tag{E34}$$

where

$$Q_{tot} = \dot{m} c_p (T_i - T_f) \tag{E35}$$

Since the total flow rate and specific heat are constant, reduction in total heat-rejection rate means that the fluid temperature difference between the tube inlet and the tube outlet has to be decreased. The change in the inlet and exit temperatures in the radiator panel can be made proportional to the heat-rejection rates from the respective headers according to the relation

$$\frac{T_i - T_{i,P}}{T_{f,P} - T_f} = \frac{Q_{i,H}}{Q_{o,H}} \tag{E36}$$

These new tube terminal temperatures $T_{i,P}$ and $T_{f,P}$ and new heat-rejection rate (eq. (E34)) can now be used in the program to determine the new panel dimensions.

APPENDIX F

RADIATOR WEIGHT

The total radiator weight consists of the tube weight, fin weight, header weight, and liquid content weight:

$$W = W_t + W_F + W_H + W_I \tag{F1}$$

The weight of the emissivity coating was neglected in this analysis. For radiators that use gas as a working fluid, the fluid content weight is negligible and not considered.

The tube weight is obtained from

$$W_t = \pi\left[\rho_t\delta_a(D_{in} + 2\delta_c + \delta_a) + \rho_c\delta_c(D_{in} + \delta_c)\right]NZ \tag{F2}$$

which includes the weight of the armor and liner. The tube wall thickness δ_a and liner thickness δ_c are obtained from equations (B1) and (B5), respectively. The densities of the armor and liner materials ρ_a and ρ_c are program inputs (table I). The product NZ is obtained from equation (B3).

The fin weight is obtained from

$$W_F = 2\rho_F LtNZ \tag{F3}$$

where the half-fin width L is given by equation (D1), and fin thickness, t is obtained from equation (D2).

The inlet and outlet header weights, which are different for radiators that use gas as a working fluid, are given in appendix E as equations (E19) and (E20), respectively. When a liquid or liquid metal is used as the working fluid, the inlet and the outlet headers are the same in size and shape. The combined header weight is given by equation (E34).

The weight of the liquid content in the liquid and liquid metal radiators was obtained from the relation

$$W_I = \frac{\pi}{4}\rho_L\left[2D_{L,H}^2H_L + D_{in}^2(NZ)\right] \tag{F4}$$

APPENDIX G

GENERATION OF MINIMUM WEIGHT CURVES FOR BRAYTON CYCLE EXAMPLE

Of the three radiator illustrative examples discussed in the text of this report, the Brayton cycle radiator used the fewest tubes. This facet of the design produced some difficulty in determining the parameters defining the minimum weight radiator not encountered with the Rankine or secondary cooling examples, because the computer program required that the number of tubes be an integer. It will be recalled that in appendix C after the tube length Z required for the prescribed pressure drop was determined, the quotient of NZ divided by Z was formed. The result was rounded off to the next higher integer, labeled N, the number of tubes in the radiator.

The difficulty referred to in the preceding paragraph became apparent when a curve of radiator weight against profile ratio for a constant conductance parameter, such as figure 7 (p. 18), was plotted for the Brayton cycle radiator. It was observed that there were discontinuities in the curve such that a well-defined minimum could not be established. These discontinuities shown in figure 34 occurred whenever the range of values of L/R_o covered required a change in the number of radiator tubes to match the heat-transfer and pressure drop requirements. The problem was to determine the minimum of the weight curve at constant λ_1. Since this minimum occurred right at a discontinuity, it was necessary to determine L/R_o at the discontinuity (see circle in fig. 34) by the following method.

The computer program was rerun for the same constant λ_1 and a group of closely spaced L/R_o ratios in the vicinity of the minimum radiator weight. For convenience, a parameter $(NZ)/Z - (N - 1)$ was devised, and all values of L/R_o and radiator weight that corresponded to a single value of N were

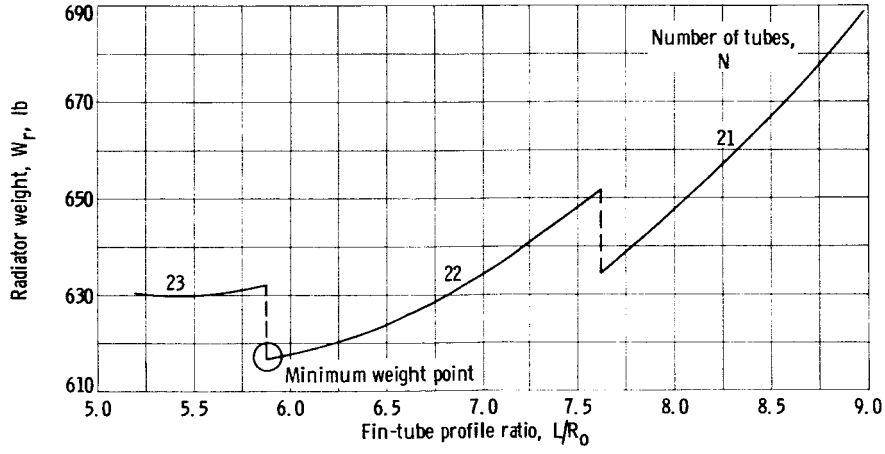

Figure 34. - Variations of total weight with fin-tube profile ratio and number of tubes at constant tube inside diameter (1 in.) and initial conductance parameter (1.0) for Brayton cycle radiator example. Power level, 8 kilowatts. (See table I for operating conditions.)

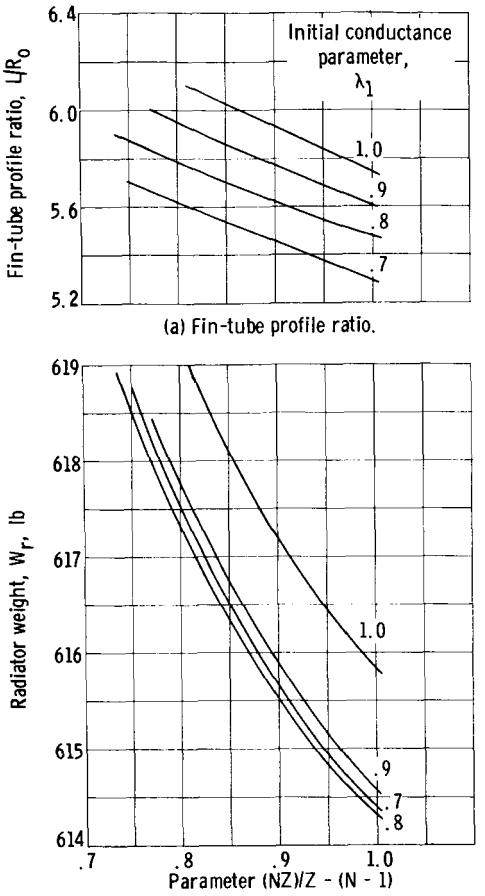

Figure 35. - Variations of total weight and fin-tube profile ratio with parameter (NZ)/Z - (N - 1) at constant tube inside diameter (1 in.) for Brayton cycle radiator example. Power level, 8 kilowatts. (See table I for operating conditions.)

plotted against this parameter for each value of λ_1, as illustrated in figure 35. This parameter was chosen because the discontinuity was defined when the parameter took on a value of 1, and because the range of the parameter was limited to values between 0 and 1 for each value of N. The ordinate values corresponding to an abscissa value of 1 then defined the minimum radiator weight and L/R_o required for minimum weight at each value of λ_1. The minimum weight curve for each tube diameter could then be drawn by plotting the minimum weights against the corresponding L/R_o ratios thus determined for each λ_1.

REFERENCES

1. Lieblein, Seymour: Special Requirements on Power Generation Systems for Electric Propulsion. Electric Propulsion for Spacecraft. NASA SP-22, 1962.

2. Walker, C. L.; Smith, C. R.; and Gritton, D. G.: Weight Optimization of Heat Rejection Systems for Space Applications. Proc. 1960 Heat Transfer and Fluid Mech. Inst., Stanford Univ. Press, 1960, pp. 244-259.

3. Krebs, Richard P.; Winch, David M.; and Lieblein, Seymour: Analysis of a Megawatt Level Direct Condenser-Radiator. Power Systems for Space Flight. Vol. 11 of Prog. in Astronautics and Aeronautics, Academic Press, Inc., 1963, pp. 475-504.

4. Haller, Henry C.: Analysis of a Double Fin-Tube Flat Condenser-Radiator and Comparison with a Central Fin-Tube Radiator. NASA TN D-2558, 1964.

5. Krebs, Richard P.; Haller, Henry C.; and Auer, Bruce M.: Analysis and Design Procedures for a Flat, Direct-Condensing, Central Finned-Tube Radiator. NASA TN D-2474, 1964.

6. Cooke, D. H.; Mayer, M. S.; and Thompson, C. A.: Space Power Plant Study. Prog. Rept. 2, WANL-PR(B)-007, Westinghouse Electric Corp., Feb. 20, 1963.

7. Denington, R. J., et al.: Space Radiator Study. Rept. No. ER-4544, Thompson Ramo Wooldridge, Inc., 1962.

8. Schreiber, L. H.; Mitchell, R. P.; Gillespie, G. D.; and Olcott, T. M.: Techniques for Optimization of a Finned-Tube Radiator. Paper 61-SA-44, ASME, 1961.

9. Stone R.; and Coombs, M. G.: Large Space Radiators. Paper Presented at IAS Prop. Meeting, Cleveland (Ohio), Mar. 7-8, 1963.

10. Lubin, Barry T.; and Trusch, Raymond B.: Prediction of Space Radiator Performance. Paper 63-AHGT-85, ASME, 1963.

11. Mackay, D. B.; and Bacha, C. P.: Space Radiator Analysis and Design. TR 61-30, pt. 1, Aeronautical Systems Div., Apr. 1, 1961.

12. Rubin, Irving; and Imber, Murray: Optimization Study of Space Radiators. AIAA J., vol. 2, no. 2, Feb. 1964, pp. 353-358.

13. Anderson, R. C.; and Henderson, B. J.: A Parametric Survey of Tube and Fin Type Radiators. Rept. No. LAMS-2793, Los Alamos Sci. Lab., Oct. 1962.

14. French, Raymond, J., Jr.: Analysis and Experimental Verification of Space Radiator Performance. Paper No. 845B, SAE-ASME, 1964.

15. Glassman, A. J.; Krebs, R. P.; and Fox, T. A.: Brayton Cycle Nuclear Space Power Systems and Their Heat Transfer Components. Paper No. 57, A.I.Ch.E., 1963.

16. Lieblein, Seymour: Analysis of Temperature Distribution and Radiant Heat Transfer Along a Rectangular Fin of Constant Thickness. NASA TN D-196, 1959.

17. Loeffler, I. J.; Lieblein, Seymour; and Clough, Nestor: Meteoroid Protection for Space Radiators. Power Systems for Space Flight. Vol. 11 of Prog. in Astronautics and Aeronautics, Academic Press, Inc., 1963, pp. 551-579.

18. Sparrow, E. M.; Jonsson, V. K.; and Minkowycz, W. J.: Heat Transfer from Fin-Tube Radiators Including Longitudinal Heat Conduction and Radiant Interchange Between Longitudinally Nonisothermal Finite Surfaces. NASA TN D-2077, 1963.

19. Knudsen, James G.; and Katz, Donald L.: Fluid Dynamics and Heat Transfer. McGraw-Hill Book Co., Inc., 1958.

20. Eckert, E. R. G.; and Drake, Robert M., Jr.: Heat and Mass Transfer. Second ed., McGraw-Hill Book Co., Inc., 1959.

21. Sparrow, E. M.; and Eckert, E. R. G.: Radiant Interaction Between Fin and Base Surfaces. J. Heat Transfer (ASME Trans.), ser. C, vol. 84, no. 1, Feb. 1962, pp. 12-18.

22. Auer, Bruce M; and Saule, Arthur V.: Program Details for Design of Sensible Heat Space Radiators, NASA TN D-2840, 1965.

23. Weatherford, W. D., Jr.; Tyler, John C.; and Ku, P. M.: Properties of Inorganic Energy-Conversion and Heat-Transfer Fluids for Space Applications. TR 61-96, WADD, Nov. 1961.

24. Hatton, Roger E.: Introduction to Hydraulic Fluids. Reinhold Pub. Corp., 1962.

25. Svehla, Roger A.: Estimated Viscosities and Thermal Conductivities of Gases at High Temperatures. NASA TR R-132, 1962.